THE ASTROPHYSICAL JOURNAL, 382:617–635, 1991 December 1

OPTICAL EXCESS EMISSION IN T TAURI STARS

PATRICK HARTIGAN,[1] SCOTT J. KENYON,[2,3] LEE HARTMANN,[2] STEPHEN E. STROM,[1,3] SUZAN EDWARDS,[1,3]
ALAN D. WELTY,[1,4] AND JOHN STAUFFER[2,3]

Received 1991 March 11; accepted 1991 May 24

ABSTRACT

We present a set of simultaneous high-resolution spectroscopic and spectrophotometric observations of 22 K7–M1 T Tauri stars in the Taurus-Auriga dark cloud. Analysis of the high-resolution data makes it possible to separate the optical excess ("veiling") emission from the photospheric fluxes in these stars. The amount of optical excess emission at 5500 Å ranges from undetectable ($\lesssim 10\%$ of the photosphere) to as much as 10 times the photospheric flux in the most extreme objects. We use the spectrophotometry to derive improved reddening corrections and determine the spectral energy distributions of the excess emission between 3500 and 8400 Å. Spectra of the excesses are flat in F_λ or rise slowly toward the blue at optical wavelengths, and most objects have a Balmer emission jump. The optical excess emission can contribute significantly to the total flux in both the V and R passbands, and the excesses have caused previous estimates of the visual extinction to be as much as 50% too low for several T Tauri stars. New values for the stellar luminosities of the program objects do not differ significantly from those obtained from near-infrared studies.

Simple models indicate that the optical excesses arise from regions with densities $\sim 10^{14}$ cm^{-3}, temperatures of ~ 9000 K, optical depths between ~ 0.2 and 5, and covering factors of $\sim 5\%$ of the stellar surface area. The mass accretion rates inferred from the excesses are typically $\sim 10^{-7}\ M_\odot$ yr^{-1}. Disk models for the near-infrared excesses indicate that accretion energy and reprocessed light from the central star contribute roughly equally to the near-infrared excesses of objects with moderate optical excesses. Our observations are consistent with the idea that optical excess emission in T Tauri stars comes from the boundary layer of an accretion disk.

Subject headings: spectrophotometry — stars: accretion — stars: pre–main-sequence

1. INTRODUCTION

In the past decade, observations from millimeter wavelengths through the ultraviolet have indicated that dense circumstellar disks are common among newly formed low-mass stars. Roughly one-half of all known solar-type pre–main-sequence stars (the so-called classical T Tauri stars) radiate more flux at infrared wavelengths than expected from extrapolations of their optical photospheric colors, and these infrared excesses have the broad spectral energy distributions expected from circumstellar disks (Rucinski 1985; Adams, Lada, & Shu 1987; Kenyon & Hartmann 1987). Observations of T Tauri stars at far-infrared and millimeter wavelengths also show excesses that are consistent with a disk interpretation (Beckwith et al. 1990; Adams, Emerson, & Fuller 1990). Additional indirect evidence for disks around classical T Tauri stars comes from observations of optical forbidden lines, where the lack of redshifted components to the line profiles has been interpreted as resulting from occultation of the receding portion of a stellar wind by a dense circumstellar disk (Appenzeller, Jankovics, & Östreicher 1984; Edwards et al. 1987). The relationship between circumstellar disks and winds has not been settled, but disk accretion provides a convenient energy source for driving the bipolar outflows and optical jets observed around many young stars.

In addition to infrared excess emission, many T Tauri stars also possess excess emission at optical wavelengths. The absorption lines in classical T Tauri stars are not as deep as those in weak-lined T Tauri stars of the same spectral type (weak-lined T Tauri stars are objects without strong Balmer emission lines and infrared excesses; Walter et al. 1988; Strom et al. 1989). This phenomenon, known as "blue veiling" because the effect can be particularly large at blue optical wavelengths where the photospheric lines often vanish completely in low-resolution spectra, was once thought to occur because emission from an active chromosphere "filled in" the deepest absorption features. Another possibility, initially proposed by Lynden-Bell & Pringle (1974), is that material from a disk accretes onto a slowly rotating stellar photosphere and deposits its kinetic energy in a boundary layer between the star and the disk (T Tauri stars typically rotate a factor of 10–20 slower than breakup speed; Hartmann et al. 1986, and Bouvier et al. 1986). The boundary layer should be considerably hotter than the stellar photosphere, so the excess continuum emission from the boundary layer at optical and ultraviolet wavelengths will cause the photospheric lines of the underlying T Tauri star to appear veiled.

An analysis of high-resolution spectra of BP Tau by Hartigan et al. (1989, hereafter Paper I) showed that the optical excess emission was caused by a continuum, with only a few emission lines superposed. Basri & Batalha (1990) found blue continuum excesses in a number of T Tauri stars while analyzing Hamilton echelle data and concluded that the results were consistent with an accretion disk model. An accretion disk model can account for the *IUE* observations of Herbig &

[1] Five College Astronomy Department, University of Massachusetts, Amherst, MA 01003.
[2] Harvard-Smithsonian Center for Astrophysics, Mail Stop 16, 60 Garden Street, Cambridge, MA 02138.
[3] Visiting Astronomer, Kitt Peak National Observatory, National Optical Astronomy Observatories, which is operated by Associated Universities for Research in Astronomy Inc. (AURA) under cooperative agreement with the National Science Foundation.
[4] Department of Astronomy and Astrophysics, Pennsylvania State University, University Park, PA 16802.

Goodrich (1986), who found substantial UV excess emission in several classical T Tauri stars, and for estimates of large excess emission at optical wavelengths (Bertout, Basri, & Bouvier 1988; Basri & Bertout 1989). The recent demonstration that optical excess emission in young stars is always accompanied by infrared excess emission (Hartigan et al. 1990) also lends support to a boundary layer interpretation of the optical/UV excesses. A correlation between Hα emission and veiling found by Hartigan et al. (1990) and Basri & Batalha (1990) indicates that boundary layer emission, and therefore disk accretion, is related to outflows from young stars.

Precise measurements of optical excess emission in T Tauri stars provide critical information about the physical properties of circumstellar disks and their boundary layers. In simple disk models the kinetic energy dissipated as material accretes from the disk onto the stellar surface is radiated as optical and ultraviolet emission from the boundary layer. Hence, optical observations of boundary layer emission yield a direct estimate of the mass accretion rate through the disk. In contrast, it is difficult to obtain reliable estimates of disk accretion rates using infrared data alone. Infrared emission from a disk heated by steady accretion is usually impossible to disentangle from the emission radiated by a "passive" disk that simply absorbs and reradiates stellar energy because both processes have identical spectral energy distributions (e.g., Adams et al. 1987). It is important to establish accurate accretion rates because sufficiently rapid deposition of mass onto the central star can affect early stellar evolution. Preliminary estimates suggest that $\sim$30% of all T Tauri stars accrete rapidly enough to perturb evolutionary tracks significantly away from Hayashi track evolution (Hartmann & Kenyon 1990). Improved observational estimates of disk accretion rates are needed to clarify the behavior of evolutionary tracks of T Tauri stars in the H-R diagram, which to this point have only been calculated under the assumption of rapid spherical accretion followed by quasi-static contraction down the Hayashi track (e.g., Durisen et al. 1989).

A long-standing problem in the study of the spectral energy distributions of T Tauri stars in the determination of an accurate value for the extinction toward these objects. Reliable reddening estimates are needed in order to calculate stellar luminosities and place the objects in the H-R diagram, as well as to estimate excess luminosities in the infrared, optical, and ultraviolet regions of the spectrum. Unfortunately, it is difficult to measure the reddening toward classical T Tauri stars because the optical excess emission makes the intrinsic colors bluer than those of the photosphere. Previous studies (Cohen, Emerson, & Beichman 1989; Cabrit et al. 1989; Kenyon & Hartmann 1990; hereafter KH) have placed classical T Tauri stars in the H-R diagram by assuming that all the emission from a particular passband (e.g., V, J, H) comes from the star. We are able to isolate the photospheric flux from the total flux (and hence determine the reddening) by using spectrophotometry to measure the observed spectral energy distributon, and simultaneous high-resolution spectra to measure the excess emission at each wavelength. The amount and time scale of any variability in the optical excess emission provides an important link between accretion in T Tauri stars and the more dramatic FU Orionis outbursts, which are generally thought to be episodic events of rapid disk accretion (Hartmann & Kenyon 1985). By subtracting the optical excess continuum from the observed spectrum, we can also look for any variations in the stellar flux that might be caused by star-spot activity.

In what follows we use high-dispersion optical spectroscopy and low-dispersion spectrophotometry to investigate the nature of the optical and near-ultraviolet excess emission in a sample of 22 T Tauri stars in the Taurus-Auriga dark cloud. We can measure the amount of excess emission more precisely than has been possible in previous studies (Paper I; Basri & Batalha 1990) because our high-resolution spectra have better signal-to-noise ratios than previous work, and because we use more appropriate photospheric templates. The high-resolution spectroscopy enables us to separate the photospheric and excess components of the emission. With the aid of the simultaneous spectrophotometric observations, we can measure improved extinction correlations, stellar luminosities, excess luminosities, mass accretion rates, and intrinsic spectral energy distributions of the optical excesses for the objects in our sample. The spectral energy distributions of the excess emission constrain the optical depths, temperatures, and areal coverages of the material responsible for the optical excesses. We evaluate the consistency of these results with the predictions from a simple steady accretion disk model.

2. OBSERVATIONS

High-resolution spectra of 22 K7–M1 T Tauri stars in Taurus-Auriga were taken with the echelle spectrograph and TI CCD mounted on the 4 m telescope at Kitt Peak National Observatory. We obtained two sets of high-resolution observations—the "blue" echelle spectra (taken 1988 November 20 and 21 UT) covered the wavelength range 3983–4922 Å, and the "red" echelle data (taken 1988 November 29 and 30 and December 1 UT) spanned the interval 4942–6834 Å. The useful wavelength range of the echelle spectra for measuring optical excess emission is 4100–6730 Å. Beyond 6730 Å, terrestrial absorption features and defects on the CCD make it difficult to measure excess emission, and shortward of 4100 Å, the signal-to-noise ratio is usually too poor to measure excesses accurately. The size of the slit on the sky was $1\farcs3 \times 5\farcs3$, and the spectral resolution was 12 km s^{-1}, with a dispersion of about 5 km s^{-1} per pixel. The orders are clearly well separated in both the red and the blue. However, we did not attempt to subtract sky from the echelle data because of the small number of sky pixels available and the additional noise introduced by sky subtraction. The sky contribution is $\lesssim$5% for all program objects.

Spectrophotometric observations of the program T Tauri and standard stars were obtained 1988 November 24–December 2 (UT) with the intensified Reticon scanner (IRS) mounted on the spectrograph at the No. 2 0.9 m telescope at Kitt Peak. The program objects and background sky were measured simultaneously with two 22″ apertures separated by 60″ in R.A. Objects were beam-switched at intervals of 90–150 s during the 20–30 minute exposures to minimize differences between the two halves of the Reticon array. The IRS spectra have a resolution of $\sim$10 Å and a wavelength range of 3500–6100 Å using grating 26, or 5700–8400 Å with grating 35. The blue IRS spectra were taken on 1988 November 24–28 and 30, and December 1, and the red IRS spectra were obtained on November 29 and December 2. The photometric calibration of the IRS data is accurate to $\pm$0.03 mag. The echelle and IRS data were reduced using the NOAO/IRAF reduction packages. A journal of the observations appear in Table 1.

We took care to ensure that the red echelle spectra (November 29 and 30, and December 1) and the IRS spectrophotometry for the program T Tauri stars were *simultaneous* to

TABLE 1

JULIAN DATES OF OBSERVATIONS (2,447,400 + date)

	Spectrophotometery		Echelle	
Object	Red	Blue	Red	Blue
AA Tau	97.84	96.75	96.74; 97.82	85.84; 86.76
BP Tau	94.69	95.70	95.69	85.76; 86.73
CI Tau	97.77	96.86	96.82	–
CW Tau	–	–	–	85.96
DF Tau	94.71	92.76; 96.73	96.70	85.89
DG Tau	94.73	92.78; 93.69; 95.85	95.84	85.71
DI Tau	97.92	–	97.92	–
DK Tau	97.71	96.83	96.78	–
DL Tau	94.77; 97.87	92.90; 95.80	95.78; 97.86	–
DN Tau	94.78	95.79	95.76	–
DQ Tau	–	–	97.90	–
DR Tau	94.91	92.82; 93.84; 95.91	95.92	85.81
DS Tau	–	–	–	86.83
GG Tau	94.74	95.74; 96.91	95.72; 96.91	86.93
GI Tau	97.75	96.89	96.87	–
GM Aur	94.96	92.95	–	86.98
LkCa 7	97.82	93.80	97.76	86.88
LkCa 8	97.85	–	97.78	–
RW Aur	94.97	93.91; 96.95	95.99; 96.97	87.02
UY Aur	94.95; 97.96	95.96; 96.94	95.96; 96.94; 97.99	86.00
V819 Tau	97.78	96.70	97.74	–
V836 Tau	97.95	–	97.96	–

within 20 minutes (Table 1). Although blue and red spectrophotometry for our program T Tauri stars were separated by ± 1 day, scans for most objects agreed to within 5% in the area of overlap (5700–6100 Å), and are straightforward to combine into a single spectrum. Differences between red and blue IRS spectra were as large as 50% for AA Tau, the most variable T Tauri star in our sample.

3. ANALYSIS OF THE HIGH-RESOLUTION SPECTROSCOPY

Figure 1 displays high-resolution spectra of three K7/M0 stars—a heavily veiled T Tauri star (DR Tau), a T Tauri star with no continuum excess emission (LkCa 7), and a young main-sequence K7 standard star in the Hyades (VA 622). The *relative* depths of the absorption lines in the spectra are nearly the same for the three stars, indicating similar spectral types, but the photospheric absorption features are much shallower relative to the continuum in the veiled T Tauri star than they are in the standard. These data suggests that spectra of veiled T Tauri stars can be modeled by the sum of a normal stellar spectrum and a continuum excess (Walker 1987; Paper I).

High resolution ($\lesssim 1$ Å) spectroscopy can detect very weak absorption features and provides an ideal means to separate optical excess emission from photospheric fluxes in T Tauri stars (Paper I; Basri & Batalha 1990). The procedure described in Paper I to extract excess emission will also be used in this work. Briefly, each of the 30 or so echelle orders (each ~ 60 Å wide) is divided into two or three wavelength intervals, and the excess emission is determined for each interval. The difference in depth between an absorption line in the veiled T Tauri star and the same line in a standard star gives a measure of the excess emission at that wavelength. We model the spectrum of a veiled T Tauri star as a normal stellar photosphere plus an excess continuum that is flat over the ~ 15 Å width of the interval, and we determine the amount of excess emission by minimizing the χ^2_ν of the model fit. Each estimate of the excess emission represents the best fit to an entire wavelength interval. A typical wavelength interval includes five to 10 distinct

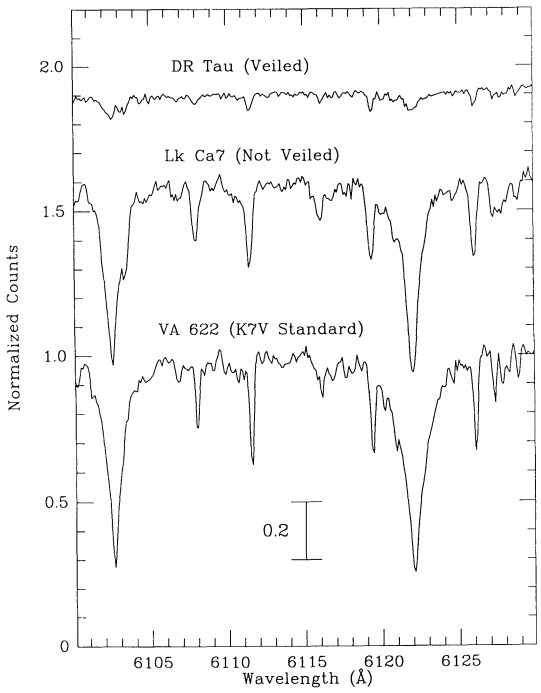

FIG. 1.—High-resolution spectra of a heavily veiled T Tauri star (DR Tau, *top*), a weak-lined T Tauri star without optical excess emission (LkCa 7, *middle*), and a main-sequence standard star (the Hyades star VA 622, *bottom*). The spectra were normalized to make the continuum levels unity and are offset from each other for clarity. The scale bar below the spectrum of VA 622 is in units of the photospheric continuum. The relative depths of the absorption lines are similar in all three objects, indicating similar spectral types, but the absorption lines in DR Tau are much shallower than those in LkCa 7 and VA 622. The absorption feature near 6103 Å is a lithium line that is present in the T Tauri stars but absent in the main-sequence standard. VA 622 has been shifted to correspond with the radial velocity of the Taurus dark cloud.

absorption features. The residuals of the fit identify any emission-line components of the excess emission. Values for χ_ν^2 usually fall between 1.5 and 3, depending on the degree of spectral type mismatch between the object and standard star (Paper I).

Estimates of the optical excess emission for different wavelength intervals have different uncertainties because of the varying number of absorption lines present with the intervals (regions without any well-defined absorption lines cannot be used to measure excess emission), and because of variations in the signal-to-noise ratio in the object and standard star spectra. However, each wavelength bin was chosen to contain several absorption lines and should have approximately the same uncertainty in the excess measurements as its neighbors. The simplest way to measure the internal precision of the method is to examine the scatter of the excess emission measured for adjacent wavelength intervals. This procedure does not address the more basic question of whether the model is a correct representation of the true physical situation (i.e., whether or not $\chi_\nu^2 > 1$). There are four sources of error in our estimates: (1) the assumption of a constant continuum excess in each interval, (2) readout noise, (3) statistical noise, and (4) mismatch between the photosphere of the standard star and that of the T Tauri star. We showed in Paper I that the optical excess in BP Tauri was primarily a continuum, with emission lines contributing less than 5% of the total excess flux. The objects in this study also have predominantly continuum excesses. Readout noise and statistical noise are known quantities and are used to produce an estimate of χ_ν^2. Differences in the photospheric line spectrum between the object and standard star are more difficult to quantify because they depend upon many unknown parameters such as the gravity, microturbulence, metallicity, and exact temperatures of the object and standard.

In Paper I we defined a model fit to be "good" if the χ_ν^2 obtained between a T Tauri star with a continuum excess and the model was lower than the χ_ν^2 obtained when comparing the standard (VA 622; a K7 V Hyades dwarf) with a star two spectral subclasses earlier (VA 68; also a Hyades dwarf). The data presented in this paper are of somewhat better quality than those presented in Paper I, so we can define a more stringent criterion for a good fit. In this paper a "good" fit is defined to be one for which the χ_ν^2 between the object and model is better than the χ_ν^2 obtained using a weak-lined T Tauri star (LkCa 7 or V819 Tau) as the object and VA 622 as the standard, a difference of one luminosity class and less than one spectral subclass. We chose to use weak-lined T Tauri stars as our primary standards to improve the match to the underlying photospheres of the program T Tauri stars. The T Tauri stars in our sample have a narrow range of spectral types (close to K7–M0), so it is possible to observe only a few weak-lined T Tauri stars as standards and still satisfy the goodness-of-fit criterion discussed above. The two most useful standard templates observed were LkCa 7 and V819 Tau, both K7–M0 weak-lined T Tauri stars.

Before we adopt V819 Tau and LkCa 7 as photospheric templates for T Tauri stars, we must demonstrate that these two weak-lined T Tauri stars have no continuum excesses. The excess derived for LkCa 7 using VA 622 as the standard appears in Figure 2*a* and scatters about zero. We present the excesses in terms of the ratio $r_\lambda = F_\lambda(\text{excess})/F_\lambda(\text{stellar continuum})$ (see Paper I for details). For example, $r = 0$ for objects without excesses, and $r = 1$ for objects that are half-veiled (i.e., photospheric absorption lines in the T Tauri star are half as deep as those in the standard template). The excess emission derived for V819 Tau using VA 622 as the standard appears in Figure 2*b* and also scatters about zero. The slope present in Figure 2*a* is not evident in Figure 2*b* and arises from differences in the depths of the absorption lines of V819 Tau and LkCa 7 (V819 Tau is slightly earlier type than LkCa 7 as indicated by its weaker TiO bands in our spectrophotometric data).

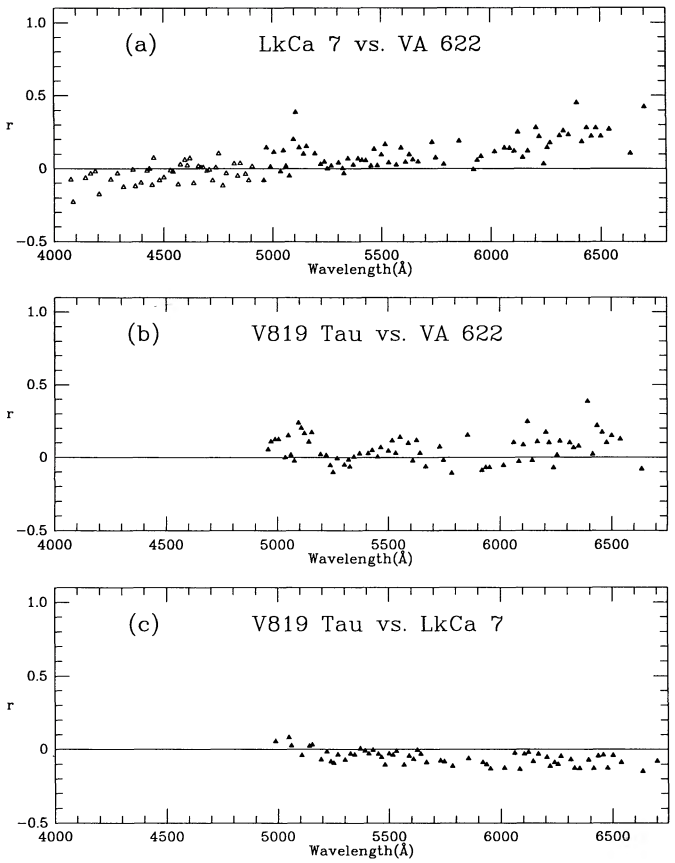

FIG. 2.—(*a*) The ratio (r) of the excess emission to the photospheric continuum as a function of wavelength. Each point represents a least-squares fit to the excess emission over a wavelength interval of 10–15 Å. The points cluster about zero, indicating that LkCa 7 has no excess continuum and can be used as a standard template for other T Tauri stars. The slope in the data arises from a slight mismatch of the spectral types of LkCa 7 and VA 622 (Lk Ca7 is somewhat later than VA 622). Solid triangles indicate observations taken with the red echelle setting, and open triangles are for the blue echelle setting. (*b*) Same as (*a*) but using V819 Tau as the object. V819 Tau has no detectable excess emission and is also a suitable standard template for T Tauri stars with excess emission. (*c*) Same as (*b*) but with LkCa 7 as the standard. The scatter is smaller in this figure than in (*a*) or (*b*) because of photospheric differences between VA 622 and the T Tauri stars. The observed offset of ~ -0.07 in r from zero indicates the degree of systematic errors expected from object and template differences of about a spectral subclass.

Most of the scatter in Figures 2*a* and 2*b* ($\sim \pm 0.15$ per point in r) is caused by differences in spectral type and gravity between the weak-lined T Tauri stars and the Hyades dwarfs. In general, the χ_ν^2 for the model fits using the weak-lined T Tauri stars as templates for the program T Tauri stars were considerably better than those using Hyades dwarfs. A detailed study of the spectral differences between the Hyades stars and the T Tauri stars is beyond the scope of this paper, although such a study could lead to improved measurements of the

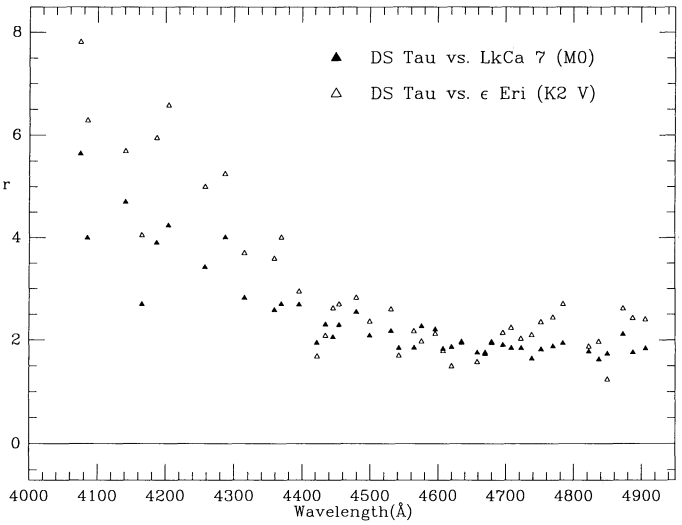

FIG. 3.—Optical excess measurements for the heavily veiled T Tauri star DS Tau using an M0 weak-lined T Tauri star (LkCa 7) and a main-sequence K2 star (ϵ Eri) as standards. The r-values differ by $\sim 30\%$ shortward of 4400 Å but are similar at longer wavelengths. The χ_ν^2 values and the scatter of the excess measurements are considerably better using LkCa 7 (a weak-lined T Tauri star) as the standard template.

abundances and gravity in young stars. In Figure 2*c* we present the r-values of the weak-lined T Tauri star V819 Tau using another weak-lined T Tauri star, LkCa 7, as the template. The fit is excellent, with χ_ν^2 averaging 1.05 and r-values of -0.06 ± 0.05. The average χ_ν^2 for the fit using LkCa 7 as the object and VA 622 as the template is much larger (2.8).

The r-values are relatively insensitive to spectral type mismatches between the object and standard of less than a spectral subclass or so at K7/M0. The r-values reflect differences in line depths relative to the continuum, and these do not vary rapidly over a spectral subclass. In Paper I we showed that the r-values obtained for BP Tau using a K7–M0 V template and those found using a K5 V template differed by only 10%–20%. Figure 3 shows the r-values for the heavily veiled T Tauri star DS Tau measured using two markedly different standard templates—a weak-lined M0 T Tauri star and a main-sequence K2 star. The amount and spectral shape of the derived excess emission is similar in the two cases. Hence, a precise match of the object and standard photospheres is less important for heavily veiled stars than for objects with small amounts of excess emission, where zero-point offsets in the excess measurements caused by an incorrect template represent a significant fraction of the excess to be measured.

Some of the objects in our sample have photospheric lines that appear rotationally broadened ($v \sin i \lesssim 10$ km s^{-1}), and for these objects we produced a standard template by artificially broadening the spectrum of LkCa 7 to the appropriate velocity in the manner described by Hartmann et al. (1986). Both optical excess emission and rotational broadening make the absorption lines in T Tauri stars appear shallower, and it is important to disentangle the two effects. The excess emission measured for UY Aur using LkCa 7 as the standard with ($v \sin i = 20$ km s^{-1}) and without (~ 12 km s^{-1} resolution) rotational broadening are presented in Figure 4. Values for the excess emission are $\sim 30\%$ lower using the rotating standard star. Uncertainties in the rotational velocity of T Tauri stars are typically 2–3 km s^{-1} (e.g., Bouvier 1990; Hartmann & Stauffer 1989), and result in $\sim 5\%$–10% uncertainties in measurements of excess emission.

4. REDDENING-INDEPENDENT MEASUREMENTS OF EXCESS EMISSION

The echelle observations can be used to determine the reddening-corrected spectral energy distribution of the excess emission *without knowing the reddening to the veiled object a priori*. The amount of veiling is measured from the depth of photospheric absorption features relative to the continuum level in a narrow wavelength interval and does not depend upon the broad-band colors of the spectrum (§ 3). Hence, the amount of veiling measured is independent of the reddening. To obtain a spectrum of the excess emission (r is defined as the *ratio* of the excess continuum to the photospheric flux), we must multiply the r-values by the flux of a dereddened photospheric template. It is not difficult to deredden the stars used as photospheric templates (LkCa 7, V819 Tau, and VA 622) because these objects do not have excess emission.

Derivation and plots of the optical excess emission as a function of wavelength are described in § 4.1, and the combination of red and blue data to produce a spectrum of the excess is presented in § 4.2. Some objects show time variability in the amount of veiling, but we postpone discussion of variability until we discuss the spectrophotometry in § 5, because without spectrophotometric data it is impossible to determine if a change in the veiling is caused by a variation in the amount of excess emission or a variation in the brightness of the stellar photosphere.

4.1. *Observations of Excess Emission*

The optical excess measurements (r_λ) obtained from our high-resolution spectra of 22 T Tauri stars appear in Figures 5*a*–5*aa*. Solid symbols denote red echelle data, and open symbols represent blue echelle data taken some 10 days earlier (a different symbol is used for each night). Only those points satisfying the goodness-of-fit criterion discussed in § 3 are shown in the figures. The standard templates were the weak-lined T Tauri stars LkCa 7 and V819 Tau (excess measurements agree to within 5% using either template). The only exception is DF Tau, an M2 T Tauri star, for which the main-sequence M2 dwarf Gl 15A was used as the standard (no M2 weak-lined T Tauri stars were available as standard templates).[5]

Except for a rise in the r-values shortward of 4500 Å, which we attribute to a drop in the photospheric flux of late K stars (see below), the excess emission is relatively flat and in some stars dominates the total monochromatic flux of the system even at wavelengths longer than Hα. These results agree well with previous studies of excess emission in T Tauri stars (Paper I; Basri & Batalha 1990). The mount of excess emission ranges from $r \lesssim 0.05$ in DI Tau (Fig. 5*i*) and V836 Tau (Fig. 5*aa*), to $r \gtrsim 2$ in DG Tau, DR Tau, DS Tau, and RW Aur (Figs. 5*h*, 5*o*, 5*p*, and 5*w*, respectively). Small excesses of a few tens of percent of the photospheric continuum are visible in several objects (DQ Tau, Fig. 5*n*; GI Tau, Fig. 5*s*; Lk Ca8, Fig. 5*u*). The excesses vary markedly over a period of 24 hours in the red echelle observations of AA Tau (Figs. 5*a* and 5*b*) and GG Tau (Figs. 5*q* and 5*r*). Over the 8–12 day interval between the red

[5] Although Cohen & Kuhi (1979) list DF Tau as M0.5, Herbig (1977) assigns it a spectral type of M3, consistent with the TiO band strengths in our data.

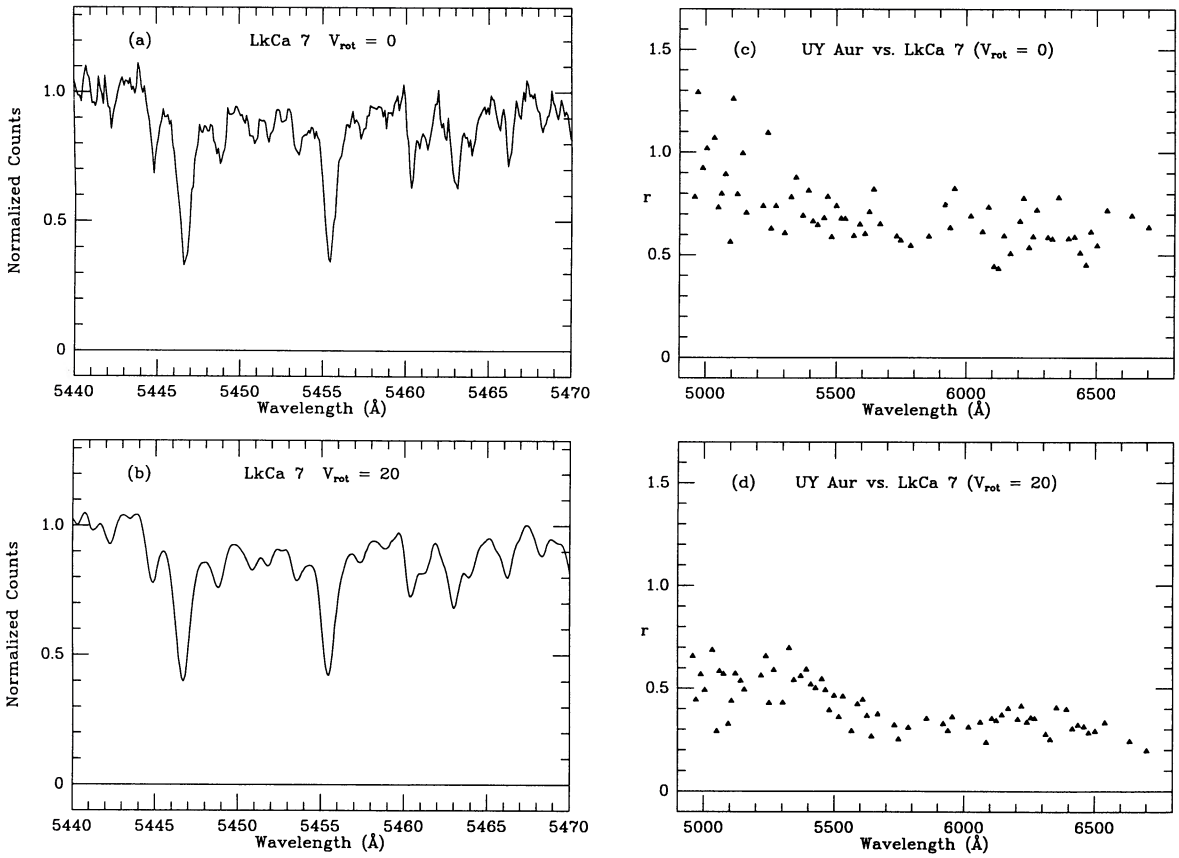

FIG. 4.—(*a*) Echelle spectrum of LkCa 7 with no rotational broadening. The spectra have ~ 12 km s^{-1} resolution. (*b*) Same as (*a*) but with a rotational broadening of $v \sin i = 20$ km s^{-1}. Rotation smooths the lines and reduces the line depth with respect to the continuum. (*c*) Optical excess emission derived for UY Aur using LkCa 7 without rotational broadening as the template. (*d*) Same as (*c*) but with LkCa 7 rotationally broadened by 20 km s^{-1}. The measured values of the excess emission are lower in (*d*) than in (*c*) because the lines in the rotating template are shallower relative to the continuum than those in the nonrotating template. The rotational velocity of UY Aur is 19 ± 3 km s^{-1}.

and blue echelle data, most objects exhibit noticeable changes in the amount of veiling.

4.2. *Conversion of Veiling Measurements to Relative Fluxes*

We must multiply the *r*-values in Figure 5 by the photospheric flux of a dereddened standard template to obtain spectra of the excess emission. The reddening (A_V) toward our two primary templates LkCa 7 and V819 Tau were measured to be 0.50 and 0.95, respectively, by comparing their spectra with a spectrum synthesized of observations of the K7 V–M0 V stars VA 622, Gl 488, Gl 851.5, and Gl 390. The Gliese (Gl) stars, located less than 20 pc away from the Sun, are not reddened significantly, and VA 622, a member of the Hyades, was also assumed to have zero reddening. Dereddened low-resolution spectra of V819 Tau and LkCa 7, are shown in Figure 6*a*. The data are normalized to make the flux of the photosphere unity at 5500 Å and are offset for clarity. The TiO features are slightly deeper in LkCa 7 than they are in V819 Tau, but the two spectra are otherwise very similar.

Spectral energy distributions for objects with both red and blue veiling measurements were combined by multiplying the *r*-values from the blue echelle data by a constant to make the red and blue results agree in the region of overlap between the two data sets. Spectral energy distributions for objects in Figure 5 with definite nonzero *r*-values are plotted in Figures 7*a*–7*w* (DF Tau is not shown because we do not have a reliable M2 spectrophotometric template). The excesses are generally flat in F_λ, with a few objects such as BP Tau exhibiting a gradual linear rise toward blue wavelengths. In contrast, the photospheric fluxes from M0 stars decrease sharply at blue optical wavelengths (Fig. 6*a*). Thus, the upturn in the *r*-values at wavelengths $\lesssim 4500$ Å in Figure 5 is caused by the decrease of the photospheric flux at these wavelengths, rather than an increase in the flux of the excess emission. Linear fits to the excess flux as a function of wavelength appear as solid lines in Figure 7 and the fits are listed in Table 2.

Although measurements of veiling are fairly insensitive to the spectral type of the template (Fig. 3 and § 2), the conversion of veiling to excess flux requires precise spectral classification because the excess flux measurements are calculated from the product of the veiling measurements and the dereddened spectrum of the photospheric template. The spectral energy distributions of late K stars differ significantly from those of early M stars at visual wavelengths (the Wien portion of the Planck function). The ratio of the dereddened spectrum of LkCa 7 to the dereddened spectrum of V819 Tau in Figure 6*b* exhibits a small slope and is indicative of the errors present in the slope of the excess emission because of reddening uncertainties in the standard templates. Objects in our study with $r(5500 \text{ Å}) \lesssim 1$ are unlikely to have been misclassified by more than a spectral subclass, because their low-resolution spectra show TiO absorption bands in the strength expected for a K7 or M0 spectral type. However, it is difficult to classify the photospheres of heavily veiled objects because of their weak absorp-

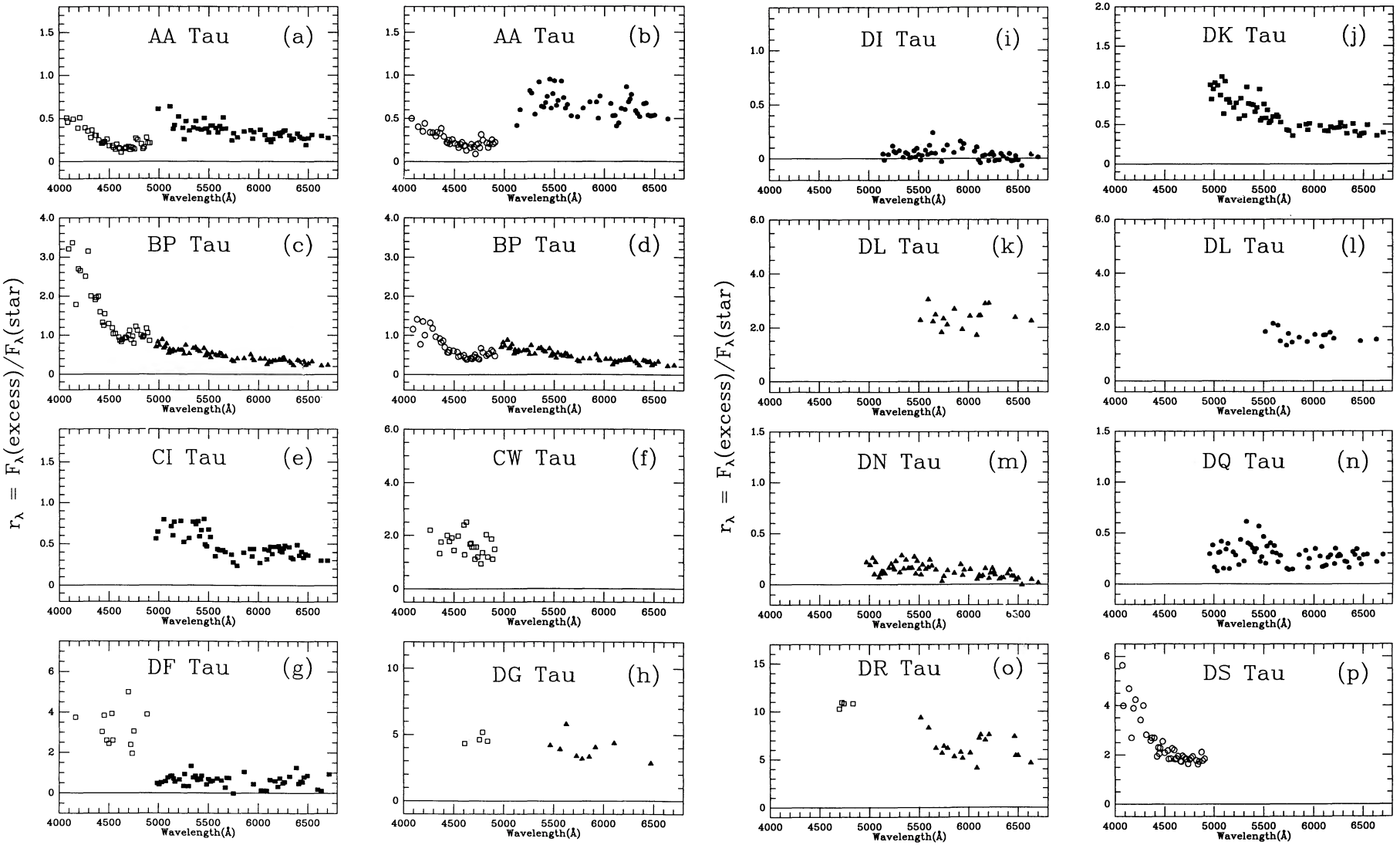

FIG. 5.—The ratio r_λ of the excess emission in our program T Tauri stars to the photospheric flux as a function of wavelength. The open symbols represent blue echelle data (squares and circles were taken November 20 and 21 UT, respectively), and solid symbols red echelle data (triangles, squares, and circles were taken November 29 and 30, and December 1 UT, respectively). Each point represents a least-squares fit to the excess emission based on a 10–15 Å portion of the echelle spectrum. LkCa 7 and V819 Tau were used as the photospheric templates (a main-sequence M star was used to model DF Tau). The value "r" is the ratio of the excess emission to the photospheric continuum. Several objects have r-values greater than unity, and some objects display ~30% variability in their excess emission over 24 hr intervals. The upturn in the r-values shortward of 4500 Å is caused by a decreasing photospheric flux at these wavelengths (cf. Fig. 6).

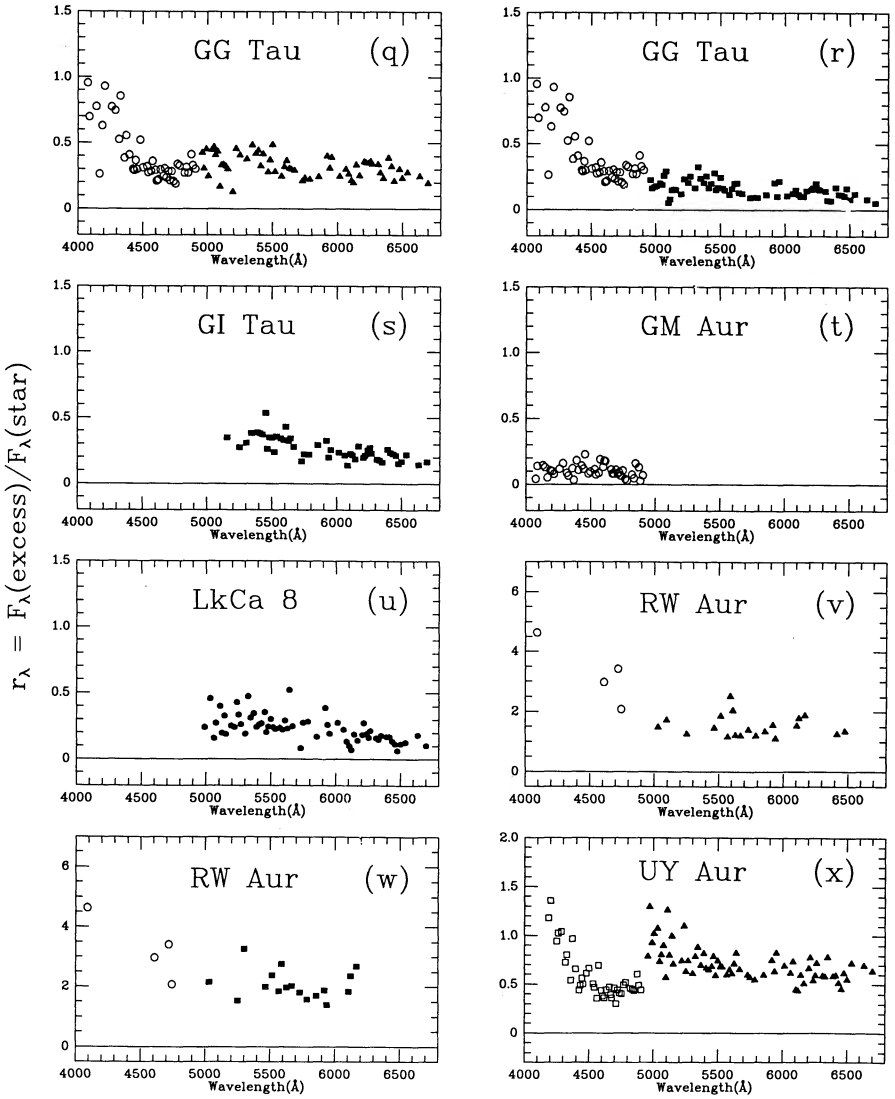

FIG. 5—*Continued*

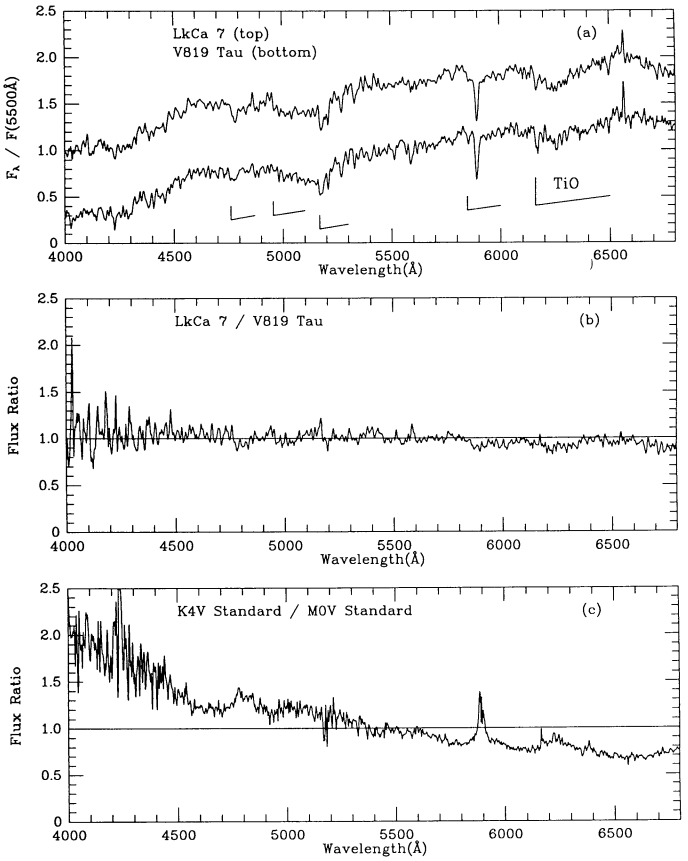

FIG. 6.—(*a*) Dereddened spectra of the photospheric template stars V819 Tau and LkCa 7 normalized to unity at 5500 Å. The spectrum of LkCa 7 has been offset vertically by 0.7 for clarity. Prominent TiO bandheads are indicated. The fluxes of these objects drop noticeably at wavelengths shorter than 4500 Å. (*b*) Ratio of the two spectra in (*a*). The ratio shows a small negative slope, which is indicative of the uncertainty in the slopes of the flux plots (Fig. 7) caused by errors in the reddening corrections applied to the standard templates and by uncertainties in the spectral type of one spectral subclass. (*c*) Same as (*b*) but for a K4 V standard and an M0 V standard. A classification error of this magnitude causes a significant error in the slope of flux plots. The classification of the objects in our sample should be accurate to within a spectral subclass.

tion features (but see Basri & Batalha 1990). As an example of errors which might result from gross misclassification, we present the ratio of the spectrum of a K4 V standard to that of a M0 V standard in Figure 6*c* (the K4 V object is from Jacoby, Hunter, & Christian 1984, and the M0 V object is our synthesized standard). If the excess emission from a T Tauri star were actually flat in F_λ but the spectral type were erroneously classified as K4 instead of M0, then the calculated spectrum for the excess emission would have the spurious slope shown in Figure 6*c*.

5. REDDENING, STELLAR LUMINOSITIES, SPECTRA OF THE EXCESS EMISSION, AND VARIABILITY

The reddening toward T Tauri stars without excess continuum emission can be found by the usual procedure of comparing the observed colors with those expected from an unreddened photosphere of the same spectral type as the star, and applying a standard reddening law. This procedure *fails* for T Tauri stars with excess emission because the intrinsic color of these objects becomes bluer by an unknown amount as the excess emission increases relative to the photospheric flux.

The combination of high spectral resolution spectroscopy and spectrophotometry enables us to separate the photospheric and excess fluxes in T Tauri stars and to derive the reddening to T Tauri stars with moderate amounts of excess emission. The high-resolution data are used to determine the amount of excess emission relative to the photospheric flux at a given wavelength (§ 4). The subtraction of the correct amount of excess emission from the spectrophotometric data leaves only the photosphere, and comparison of the observed photospheric spectrum with the spectrum of a standard template yields an estimate of the reddening. We can then correct the observed spectrophotometry for reddening and subtract out the photospheric template to obtain a spectrum of the excess emission (corrected for reddening) over the entire range of the spectrophometry, including blueward of the Balmer jump. Objects with multiple observations can be analyzed to determine whether the photosphere or the excess emission is the principal cause of any variability.

We describe the method used to obtain the reddening from the spectrophotometry and the echelle data in § 5.1, and present estimates of the reddening and stellar luminosities for the program objects in §§ 5.2 and 5.3, respectively. Spectra of the excess emission are discussed in § 5.4, and the variability of the sources is summarized in § 5.5.

5.1. *Separation of the Stellar and Excess Components of the Spectrophotometry*

We used the following procedure to estimate the excess spectrum and the reddening from a set of simultaneous spectrophotometric and echelle observations. First we determine the ratio R_λ of the excess emission to the average photospheric flux over the wavelength interval of interest (the R_λ values are typically 10%–20% larger than the r_λ values because the photospheric continuum level is always somewhat larger than the average photospheric flux over a wavelength interval; Paper I). Let F_λ(std) be the observed low-resolution (spectrophotometric) spectrum of the standard template. The actual dereddened spectrum of a T Tauri star is assumed to be the sum of the photospheric spectrum, given by the standard template, and an excess continuum, given by the echelle measurements. The model spectrum of the T Tauri star is then

$$F_\lambda(\text{model}) = (1 + R_\lambda)F_\lambda(\text{std}) , \quad (1)$$

where R_λ is measured from the linear fits to the excess fluxes shown in Figure 7.

If the standard template matches the underlying photosphere well, then the major difference between the model and observed spectrophotometry of the T Tauri star and the standard should be a slope caused by interstellar reddening. The amount of reddening can be evaluated by dividing the object spectrum by the model spectrum:

$$d_\lambda = \frac{F_\lambda(\text{TTS})}{F_\lambda(\text{model})} \quad (2)$$

The slope of d_λ as a function of λ provides a measure of the interstellar reddening, E_{B-V}, for a standard interstellar extinction curve (Savage & Mathis 1979).

The dereddened object spectrum and the model spectrum differ by a scale factor s (independent of wavelength) that depends on the ratio of the solid angles subtended by the

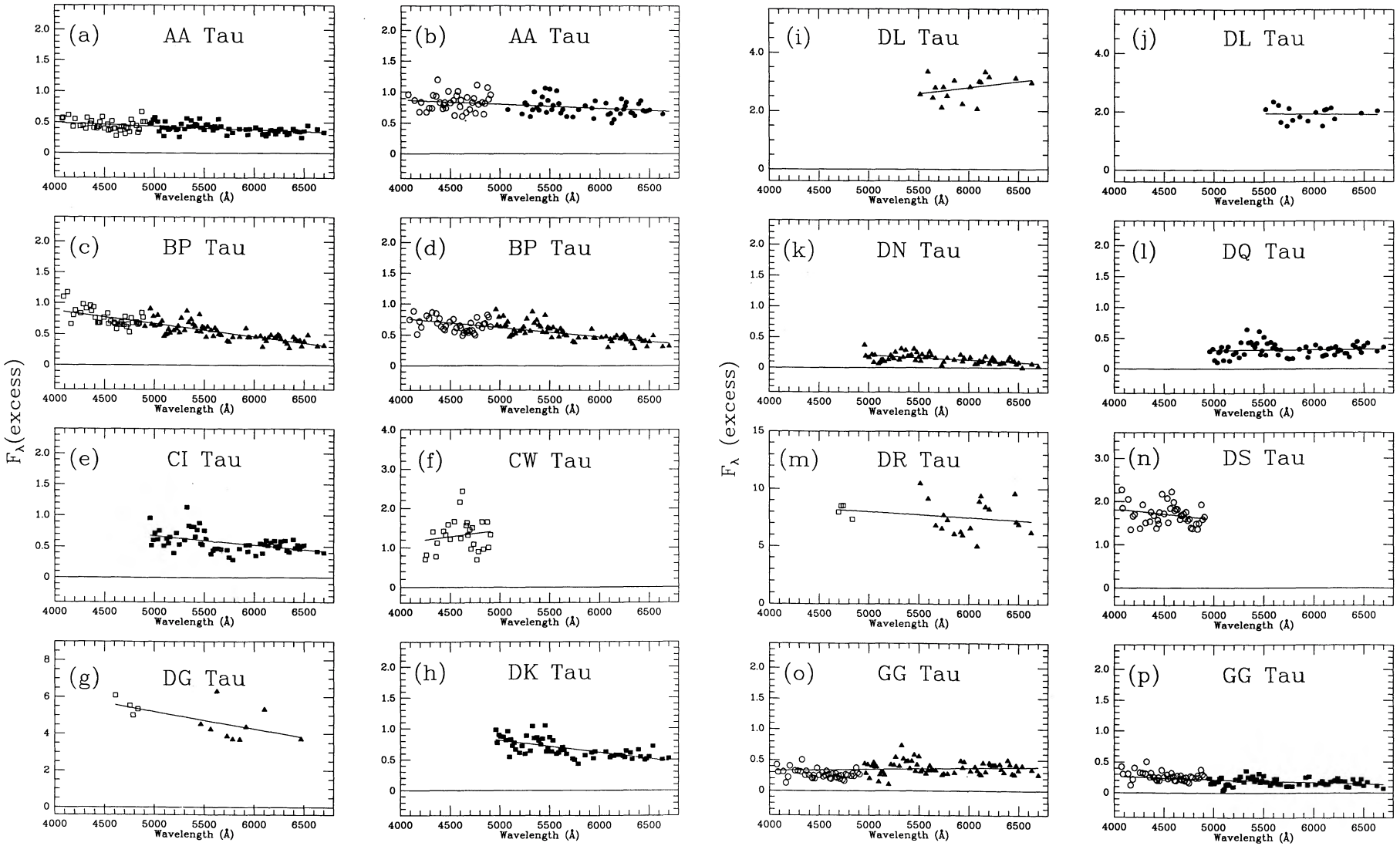

FIG. 7.—The continuum excess emission for the program T Tauri stars obtained from the echelle data. The data are normalized by the photospheric template flux at 5500 Å (dereddened low-resolution spectra of the photospheric templates LkCa 7 and V819 Tau are displayed in Fig. 6*a*). Spectra of the excess emission are nearly flat in F_λ or rise gradually toward shorter wavelengths. A linear fit to the excess fluxes is shown. The open symbols represent blue echelle data (squares and circles were taken November 20 and 21 UT, respectively), and the solid symbols indicate red echelle data (triangles, squares, and circles were taken November 29 and 30, and December 1 UT, respectively). The blue echelle results were normalized to match the red echelle points at 5000 Å as described in the text. The fluxes in this figure are *independent* of the reddening toward the T Tauri star (see text).

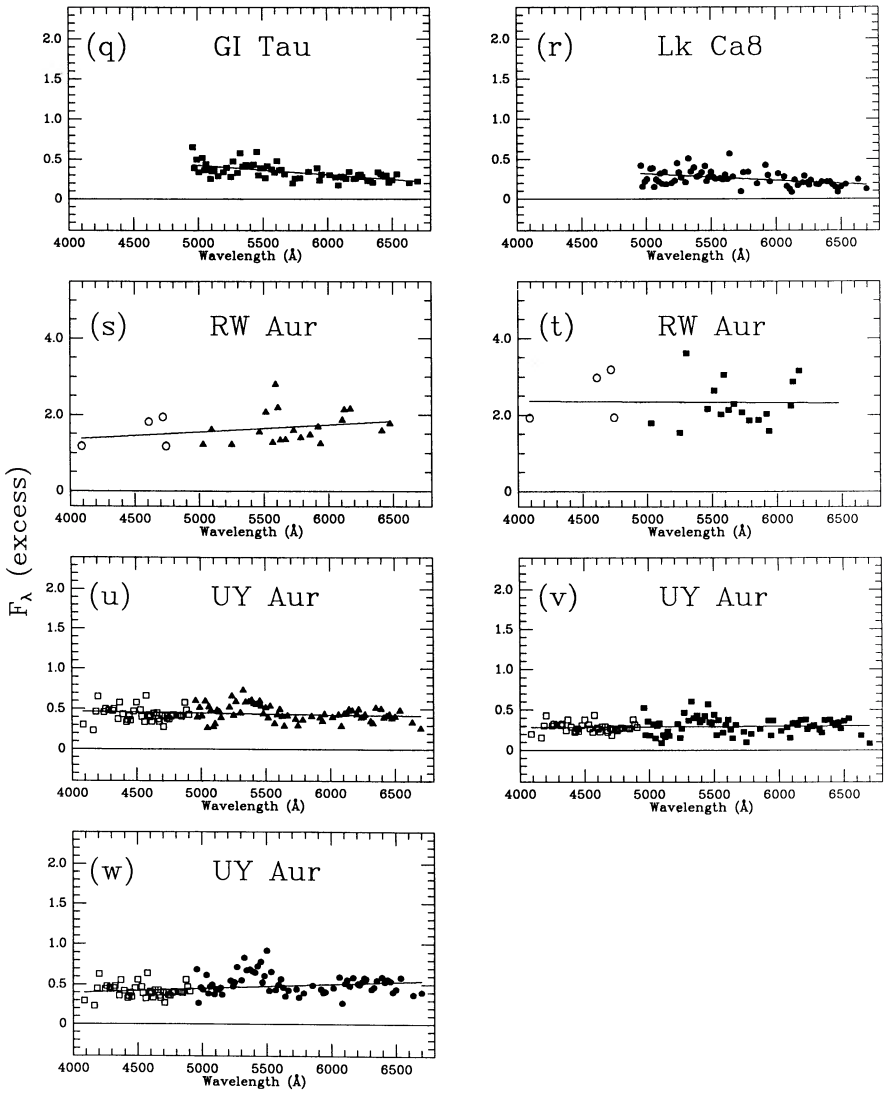

FIG. 7—*Continued*

object and standard as seen from Earth,

$$s = \frac{F_\lambda(\text{TTS, dered})}{F_\lambda(\text{model})} . \quad (3)$$

The spectrum of the underlying photosphere of the T Tauri star is then

$$F_\lambda(\text{phot}) = sF_\lambda(\text{std}) . \quad (4)$$

Finally, the spectrum of the excess emission is the difference of the dereddened spectrum and the photospheric spectrum:

$$F_\lambda(\text{excess}) = F_\lambda(\text{TTS, dered}) - F_\lambda(\text{phot}) . \quad (5)$$

The expression for the excess emission in equation (5) involves the spectral type of the stellar photosphere. Fortunately, the strength of red TiO bands is sensitive to spectral type for K7–M1 dwarfs, so it is possible to find a good estimate of the spectral type by solving for the excess emission with several different standard stars and choosing the standard for which F_λ(excess) shows no photospheric features. In practice, we used the weak-lined T Tauri stars LkCa 7 and V819 Tau as standard templates for the spectrophotometry (see also § 3). We have calibrated TiO band strengths for a small group of T Tauri stars; V819 Tau has a spectral type of K7.5, and LkCa 7 is somewhat later, and classified as M0.5.

5.2. *Reddening Results*

The optical excesses in T Tauri stars have intrinsically bluer energy distributions than the underlying stellar photospheres, so extinction corrections based on optical colors systematically underestimate the true extinction if the excess component is ignored. In Figure 8 we display the difference in A_V calculated by dereddening our spectrophotometric data according to a standard reddening law with, and without correcting for excess emission. The two estimates of the extinction typically differ by $\sim$0.7 mag at V when $R \sim 0.5$ at 5500 Å. The solid line in Figure 8 represents the error made in A_V caused by ignoring excess emission component for a model excess spectrum that is flat in F_λ and a photosphere with $T = 4000$ K. Figure 8 shows that the values of A_V calculated when $R \sim 0.2$ (such as are present for DN Tau in Fig. 7*k*) differ by as much as 0.3–0.4 from those found assuming no excess emission.

TABLE 2

VEILING, LUMINOSITIES, AND REDDENING

Object	[1]R_{5500A}	[2]Slope	[3,6]L_* ($L_\odot$)	[3,4,6]$L_{uv/opt}$($L_\odot$)	[3,6]A_V(mag)
AA Tau	0.41 ±0.07	−0.06 ± 0.01	1.3 (1.0)	0.11 (0.10)	1.3 (1.1)
AA Tau	0.77 ±0.13	−0.07 ± 0.02	0.33 (0.30)	0.06 (0.05)	1.5 (1.4)
BP Tau	0.57 ±0.10	−0.21 ± 0.01	(2.0) 1.7	(0.21) 0.19	(1.1) 0.95
BP Tau	0.54 ±0.10	−0.15 ± 0.01	(1.7) 1.3	(0.18) 0.15	(0.95) 0.65
CI Tau	0.60 ±0.14	−0.15 ± 0.04	(1.9) 1.4	(0.25) 0.18	(2.5) 2.2
[5,7]CW Tau	1.31 ±0.42	0.31 ± 0.42	–	–	–
DG Tau	4.74 ±0.77	−0.96 ± 0.38	–	–	–
DK Tau	0.71 ±0.11	−0.19 ± 0.03	(2.3) 1.9	(0.33) 0.26	(1.5) 1.3
DL Tau	2.58 ±0.39	0.42 ± 0.31	–	–	–
DL Tau	1.93 ±0.25	−0.03 ± 0.20	–	–	–
DN Tau	0.16 ±0.06	−0.08 ± 0.02	2.1 (1.9)	0.07 (0.05)	1.1 (0.95)
[7]DQ Tau	0.31 ±0.11	0.01 ± 0.03	–	–	–
DR Tau	7.7 ±1.4	−0.51 ± 0.51	–	–	–
[5,7]DS Tau	1.69 ±0.24	−0.25 ± 0.16	–	–	–
GG Tau	0.34 ±0.10	0.05 ± 0.01	(2.8) 2.4	(0.21) 0.19	(1.4) 1.3
GG Tau	0.20 ±0.07	−0.06 ± 0.01	(2.6) 2.3	(0.09) 0.10	(1.3) 1.2
GI Tau	0.37 ±0.08	−0.12 ± 0.02	(2.1) 1.5	(0.14) 0.11	(2.0) 1.7
LkCa 8	0.27 ±0.09	−0.08 ± 0.02	–	–	–
RW Aur	1.64 ±0.41	0.19 ± 0.14	–	–	–
RW Aur	2.33 ±0.60	−0.02 ± 0.25	–	–	–
UY Aur	0.44 ±0.10	−0.01 ± 0.01	(1.3) 1.0	(0.10) 0.08	(0.95) 0.7
UY Aur	0.29 ±0.09	0.01 ± 0.01	(1.3) 1.0	(0.07) 0.07	(1.1) 0.95
UY Aur	0.48 ±0.12	0.04 ± 0.02	(1.3) 1.1	(0.12) 0.11	(1.3) 1.1

NOTES.—(1) The uncertainties listed are the rms deviations of the points about the straight line fits in Fig. 7. (2) The slope of a linear fit to the excess emission in units ΔF_λ per 1000 Å. All excess fluxes are given in units of the dereddened photospheric flux at 5500 Å (see Fig. 7). (3) The two values shown for L_*, $L_{uv/opt}$, and A_V were calculated using LkCa 7 and V819 Tau, respectively, as standards. The preferred value is *not* enclosed in parentheses. (4) Observed optical excess luminosities from 3500 to 8000 Å, uncorrected for bolometric or geometric effects. (5) The r-values quoted for CW Tau and DS Tau are averages of the veiling measurements between 4000 and 5000 Å (the objects were not observed at 5500 Å). (6) We cannot estimate A_V, L_*, or $L_{uv/opt}$ for heavily veiled objects ($r \gtrsim 1$). (7) CW Tau, DQ Tau, DS Tau, and LkCa 8 were not observed spectrophotometrically at both red and blue wavelengths, so we do not calculate L_*, $L_{uv/opt}$, and A_V for these objects.

The reddening estimates, stellar luminosities, and excess luminosities for the program T Tauri stars appear in Table 2. We have calculated the stellar luminosities and reddenings only for those objects with excess emission, because standard methods for finding luminosities and reddenings (e.g., Cohen & Kuhi 1979; KH; Strom et al. 1988) are applicable to objects without excess continuum emission. We were unable to find the reddening toward heavily veiled objects (DG Tau, DL Tau, DR Tau, and RW Aur) because of larger uncertainties in the slope of the excess emission with wavelength (Figs. 5 and 6; Table 2) and the difficulty in classifying the photospheres of these objects. Also, no reddenings could be calculated for objects without both red and blue spectrophotometric observations (CW Tau, DS Tau, DQ Tau, and LkCa 8; see Table 2).

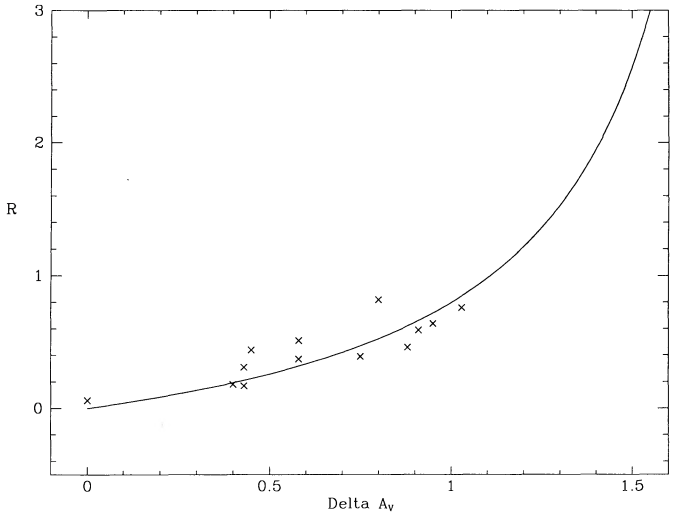

FIG. 8.—The excess emission R(5500 Å) plotted vs. the difference between the visual extinction derived from the spectrophotometry using the echelle data to measure excess emission, and that derived from the spectrophotometry assuming no excess emission. The curve represents the case of excess emission flat in F_λ added to the photospheric flux of a K7/M0 star, where the extinction is measured from the photospheric $B - V$ color.

Uncertainties in the standard templates are the primary source of error in the measurements. The differences of ~20% between the A_V values and stellar luminosities obtained using LkCa 7 as the standard and those using V819 Tau as the standard provide an indication of the uncertainties in the results. Errors in the slope of the excess emission also affect the reddening measurements, although these are unimportant except for the heavily veiled stars, where the r-values are uncertain. Our best estimates of A_V for the seven stars in Table 2 average 33% higher than those published by Cohen & Kuhi (1979), and 34% higher than those found by Strom et al. (1989) from $V - R$ colors.

5.3. *Stellar Luminosities*

A common way to measure the stellar luminosity (L_*) of a T Tauri star with excess emission is to deredden the object and then assume that the total flux at a particular wavelength arises entirely from the star. Cohen et al. (1989) used 0.44–0.67 μm to measure stellar luminosities; Cabrit et al. (1990) and Strom et al. (1989) used 0.65 μm (R); KH normalized at 1.25 μm (J), and Strom et al. (1988) chose 1.6 μm (H). We estimate L_* without making any assumptions about the spectral energy distributions of the excess emission, but we must still make extinction corrections. The stellar luminosities listed in Table 2 (ignoring AA Tau, which was highly variable, and UY Aur which is

discussed below) agree to within a mean error of 13% with the results of KH, 23% with the results of Strom et al. (1988), and 18% with the stellar luminosities reported by Cohen et al. (1989). The values of L_* from Cabrit et al. (1990) and from Strom et al. (1989) are systematically $\sim 40\%$ lower than ours. The largest discrepancy with previous studies is our measurement of $L_* = 1.0\ L_\odot$ for UY Aur, which is about a factor of 2 lower than previous estimates. This object has a flat spectral energy distribution and appears to have substantial excess emission at all wavelengths, which causes any normalization technique to overestimate the stellar luminosity (see § 6).

The excess emission (Fig. 7) often contributes significantly to the total flux at 6500 Å and is even more important at shorter wavelengths. For this reason normalizations in the near-infrared produce better estimates of the stellar luminosities than do optical normalizations, although emission from hot dust begins to contaminate the spectral energy distribution at wavelengths longer than H (see KH). Uncertainties in the reddening are also smaller at near-infrared wavelengths than they are in the optical, so that luminosities derived from infrared measurements are less uncertain than those derived from optical fluxes. At first glance it is surprising that the new values of L_* in Table 2 agree as well as they do with previous studies based on fluxes at V and R, because ignoring the excess emission leads to an underestimate in A_V of ~ 0.7 mag (Fig. 8). However, previous studies initially overestimated the stellar luminosities by ignoring the excess emission, an error that tends to cancel the effect of underestimating the reddening (Strom et al. 1989).

5.4. *Spectra of the Excess Emission*

The dereddened spectral energy distributions of the excess emission are displayed together with the dereddened spectra of the T Tauri stars in Figure 9. The excess emission is fairly flat in F_λ from 4000 to 8000 Å, in agreement with the results in Figure 7. Most objects have Balmer continuum emission shortward of 3650 Å, and reasonably strong emission lines of H I, He I, and Fe II. None of the program stars possess a significant Paschen jump at 8204 Å, but we cannot detect Paschen jumps easily from the spectrophotometry because of the small amount of excess emission present in most objects at 8204 Å.

5.5. *Variability*

Multiple sets of echelle and spectrophotometric observations of BP Tau, GG Tau, AA Tau, and UY Aur enable us to identify the primary cause of variability in these objects. The results in Table 2 show that the reddening toward these four objects remained constant to within the observational errors. Both photospheric variability *and* changes in the amount of excess emission are important in AA Tau, where the stellar flux decreased by a factor of 4 and the excess emission decreased by a factor of 2 between two sets of observations separated by 24 hr. Large amplitude variations of up to a magnitude at visual wavelengths (Vrba et al. 1989) and strong X-ray emission (Walter & Kuhi 1981) suggest that starspots cover a substantial fraction of the photosphere of AA Tau. Basri & Batalha (1990) found that the r-values at 6560 Å in AA Tau vary between 0 and 1.6, and our results confirm the variability of the excess emission in AA Tau. UY Aur and GG Tau exhibited no detectable changes in stellar luminosity, so the differences in the relative fluxes of the photosphere and the excess emission in Figure 7 result from changes in the amount of excess emission alone. The stellar and excess luminosities are similar in the two sets of BP Tau data.

6. MODELS OF THE EXCESS EMISSION, MASS ACCRETION RATES, AND THE BOUNDARY LAYER MODEL

We can infer some of the basic physical characteristics of the material producing the excess emission from the spectral energy distributions in Figures 7 and 9. The strength of the Balmer jump and the slope of the spectral energy distributions provide quantitative estimates of the optical depth, temperature, and the size of the emitting region. We describe the simple models used to compute these three parameters in § 6.1. Interpreting the emission in the context of a boundary layer model, we derive rates for mass accretion onto the star in § 6.2. The boundary layer model predicts that an accretion disk should radiate half of its energy at infrared wavelengths, and in § 6.3 we attempt to distinguish between reprocessing and accretion components of the infrared excesses for our program objects.

6.1. *Models of the Excess Emission*

The spectral energy distributions of the excess emission in Figure 9 have Balmer emission jumps and relatively flat continua at optical wavelengths. A slab of pure hydrogen gas of constant temperature and density in LTE produces a continuum spectrum, where the size of the Balmer jump depends on the optical depth of the slab and the slope of the Paschen continuum changes with both the temperature and optical depth of the slab. In this section we apply a slab model to the observations of excess emission in order to estimate the density, size, optical depth, and temperature of the material producing the excess emission.

The H^- opacity of a slab of pure H gas in LTE increases with the density, so we begin by estimating an order of magnitude for the density. The thickness of the slab should be ~ 0.01–$0.1\ R_*$ if the excess emission comes from the boundary layer of a disk (Kenyon & Hartmann 1987). The thickness of a slab needed to produce an optical depth of unity at 5550 Å (the optical depth in the Paschen continuum must be of order unity to produce a Balmer jump and a blue continuum) appears as a function of temperature in Figure 10 for several densities. The figure shows that particle densities between 10^{13} and 10^{15} cm^{-3} are appropriate for a slab model.

We can measure the temperature and optical depth of the excess emission with the aid of flux ratio diagrams which plot the height of the Balmer jump, F_{3620}/F_{4050}, as a function of the slope of the Paschen continuum, F_{5550}/F_{4050} for the dereddened excess spectra in Figure 9. Figure 11 displays these ratios for blackbodies, stellar photospheres, and our program T Tauri stars along with model ratios for particle densities of 10^{14} and 10^{15} cm^{-3}. The solutions for the optical depth and temperature obtained using $n = 10^{14}$ cm^{-3} (Fig. 11, *top panel*) do not differ significantly from those obtained using $n = 10^{15}$ cm^{-3} (Fig. 11, *bottom panel*). The pronounced dip in the locus of stellar photospheres at $5550/4050 = 0.5$ is caused by the strong Balmer absorption jump in the photospheres of A-type stars. The T Tauri stars lie on the opposite side of the blackbody line from stars (they have Balmer *emission* jumps).

A constant density slab reproduces the observed flux ratios if the gas temperatures and optical depths lie in the ranges $6000 \lesssim T \lesssim 12{,}000$ K, and $0.8 \lesssim \tau(5550\ \text{Å}) \lesssim 4$. The observed r-values provide an estimate for the ratio A/A_* of the surface area of the excess emission to the area of the stellar photo-

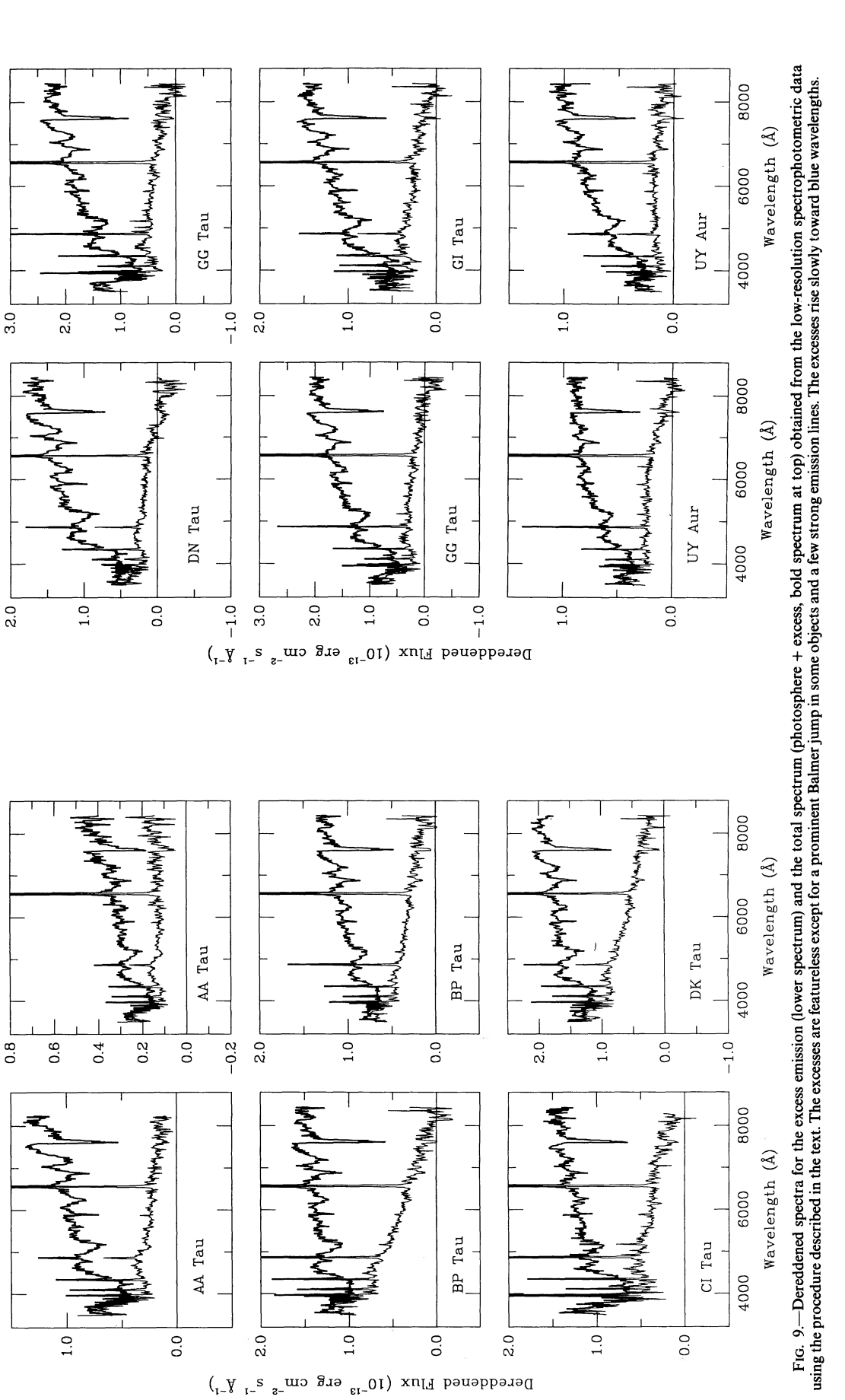

FIG. 9.—Dereddened spectra for the excess emission (lower spectrum) and the total spectrum (photosphere + excess, bold spectrum at top) obtained from the low-resolution spectrophotometric data using the procedure described in the text. The excesses are featureless except for a prominent Balmer jump in some objects and a few strong emission lines. The excesses rise slowly toward blue wavelengths.

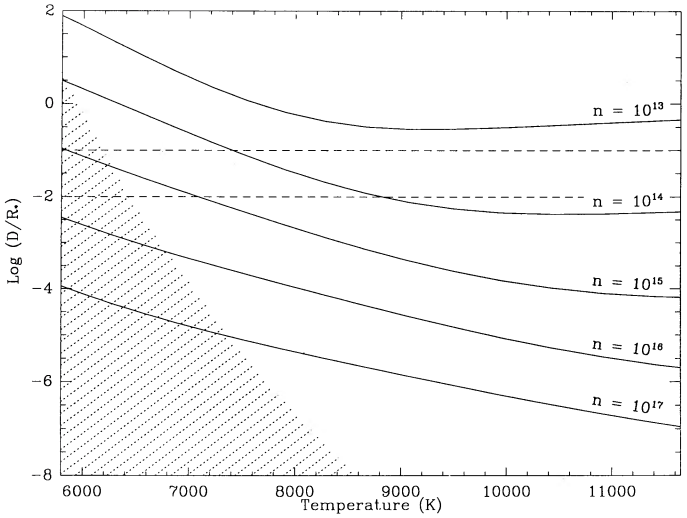

FIG. 10.—The thickness D of a slab needed to produce an optical depth of unity at 5500 Å is shown for a variety of densities. The slab models consist of pure hydrogen gas in LTE at a constant temperature and density. The density must lie between $\sim 10^{14}$ and $\sim 10^{15}$ cm^{-3} to produce optical depths of order unity at 5550 Å and slabs comparable in size to those expected from the boundary layer of a circumstellar disk ($0.01 \lesssim D/R_* \lesssim 0.1$; a region indicated by the dashed lines in the figure). Metals contribute more than 5% of the free electrons in the shaded region of the figure. Metals are unimportant in our boundary layer models, which have higher temperatures and lower densities than those within the shaded region. The stellar radius is taken as $3\,R_\odot$ in this example.

sphere. The results in Table 3 indicate that $A/A_* \sim 0.01$–0.1 for all of the objects, a value consistent with boundary layer models (Kenyon & Hartmann 1987; Bertout et al. 1988a; Basri & Bertout 1989; KH). In addition, the spectra energy distributions of the excess emission in Figure 9 are consistent with an accretion disk interpretation; boundary layers of accretion disks should have relatively featureless spectra except for Balmer continuum jumps and a few emission lines because rotational broadening will smear out even strong absorption features in a boundary layer.

The slab models are unaffected by the assumption of a pure hydrogen composition. We calculated the fraction of electrons produced by metallic ionization by solving the Saha equation for 14 elements (including Fe) with three ionization states. The region of temperature-density space where metals contribute more than 5% of the total number of free electrons is indicated by the dotted area in Figure 10, and occurs at higher densities and lower temperatures than our models for the excess emission. The slab models can be improved by using more realistic calculations that take into account the changing temperatures, ionization fraction, and densities of the emitting material. Some of the excess emission shortward of the Balmer jump could come from a stellar wind, and if a wind does contribute to the excess emission then the optical depths inferred for a slab model would increase, as would densities in the slab.

Spectrophotometric observations of heavily veiled objects are summarized in Table 4. The Balmer jump ratios (F_{3620}/F_{4050}) of the heavily veiled objects are not corrected for reddening and should increase by a factor of about 1.4 when the objects are dereddened (for $A_V \sim 2$). There is no obvious correlation between the amount of excess emission and the strength of the Balmer jump.

TABLE 3

FLUX RATIOS AND MODELS FOR PARTIALLY VEILED STARS

Object	$\frac{F_{3620}}{F_{4050}}$ [a]	$\frac{F_{5550}}{F_{4050}}$ [a]	T [b]	τ_{5550}	A/A_* [c]
AA Tau	2.69	1.10	9000	1.3	0.03
BP Tau	1.50	0.69	10000	4.0	0.04
CI Tau	2.47	0.83	13000	1.8	0.02
DK Tau	1.36	0.72	10000	4.0	0.07
GG Tau	3.63	1.75	9000	0.9	0.10
GG Tau	2.46	2.06	9000	1.3	0.04
GI Tau	1.37	0.90	8000	3.0	0.05
UY Aur	1.50	0.95	8000	2.5	0.01
UY Aur	1.94	1.49	5700	0.8	0.07

[a] Dereddened flux ratios for the excess emission. The F_{3620}/F_{4050} ratio is a measure of the Balmer emission jump, and the F_{5550}/F_{4050} ratio indicates the slope of the Paschen continuum. Errors in the observed ratios are about $\pm 10\%$ (see Fig. 11).

[b] Values for the temperature and optical depth of the excess emission are calculated from the observed flux ratios assuming $n = 10^{14}$ cm^{-3} (Fig. 11).

[c] Areal covering factor of the excess emission for $\cos i = 1/2$ and the R_* values in Table 5.

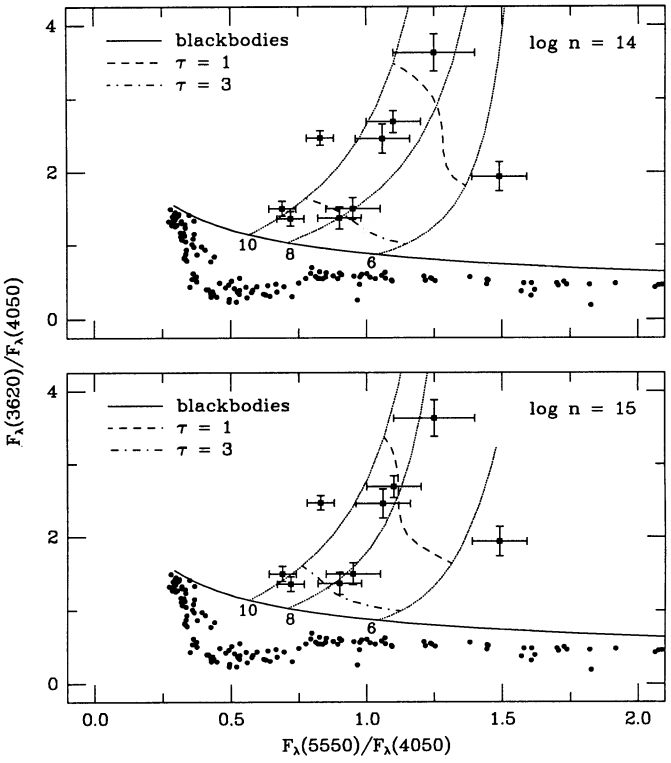

FIG. 11.—A flux ratio diagram for the excess emission in T Tauri stars. The observed flux ratios were taken from the dereddened spectra of the excess emission shown in Fig. 9. Observations of stellar photospheres from the KPNO spectral atlas (Jacoby, Hunter, & Christian 1984) are indicated by the filled circles in each panel, while blackbodies appear as a solid line. The remaining curves show flux ratios for a constant density, constant temperature, slab of solar composition in local thermodynamic equilibrium. Flux ratios for gas temperatures of 6000, 8000, and 10,000 K are drawn as dotted lines (the curves are labeled 6, 8, and 10, respectively), and ratios for constant optical depth are dashed lines ($\tau = 1$) and dot-dashed lines ($\tau = 3$). The total particle density appears in the upper right corner of each panel (the particle density affects the H^- opacity of the slab). The model can produce the observed flux ratios if the gas temperatures and optical depths lie in the ranges $6000 \lesssim T \lesssim 12{,}000$ K, and $4 \lesssim \tau \lesssim 0.8$ for particle densities between 10^{14} and 10^{15} cm^{-3}.

TABLE 4

FLUX RATIOS FOR HEAVILY VEILED STARS

Object	JD[a]	$\frac{F_{3620}}{F_{4050}}$[b]	$\frac{F_{5550}}{F_{4050}}$[b]
DF Tau	92.76	1.49	3.40
DG Tau	92.78	1.07	1.82
DR Tau	92.82	1.54	1.29
DL Tau	92.90	1.02	1.80
DG Tau	93.69	1.21	1.89
DR Tau	93.84	1.16	1.25
RW Aur	93.91	1.20	1.46
DL Tau	95.80	1.33	2.47
DG Tau	95.85	1.26	1.96
DR Tau	95.91	0.93	1.08
DF Tau	96.73	1.27	3.91
RW Aur	96.95	0.97	1.56

[a] JD of observation is 2,447,000 + the tabulated value.

[b] Observed flux ratios for the excess emission in heavily-veiled stars ($r \gtrsim 1$). Simultaneous veiling measurements exist for the last five entries in this table and are presented in Table 2. The flux ratios are *not* corrected for reddening. The F_{3620}/F_{4050} ratio is a measure of the Balmer emission jump, and the F_{5550}/F_{4050} ratio indicates the slope of the Paschen continuum. Errors are about $\pm 10\%$.

6.2. *Optical-UV Excess Luminosities and Mass Accretion Rates*

The observed reddening-corrected luminosities ($L_{uv/opt}$) for the excess emission are compiled in Table 2 and in Table 5. Assuming that the optical excesses arise from the boundary layer of an accretion disk, we can convert the observed values of $L_{uv/opt}$ to mass accretion rates as follows. The total luminosity of an accretion disk is

$$L_{total} = L_{bl} + L_{acc} + L_{rep} , \quad (6)$$

where L_{bl} is the luminosity of the boundary layer, L_{acc} is the energy released by material accreting through the disk, and L_{rep} is the "reprocessing" luminosity, generated by absorption and reradiation of energy from the central star. In the simple model for accretion onto a slowly rotating star, the boundary layer luminosity equals the disk accretion luminosity (Lynden-Bell & Pringle 1974) and is related to the mass accretion rate $\dot{M}$ by the equation

$$L_{acc} = L_{bl} = \frac{1}{2}\frac{GM_*\dot{M}}{R_*} , \quad (7)$$

where M_* and R_* are the mass and radius of the central star, respectively.

Equation (7) gives the mass accretion rate $\dot{M}$ in terms of the boundary layer luminosity L_{bl}. To obtain L_{bl} we must correct the observed luminosity $L_{uv/opt}$ for bolometric and geometric effects. For an axially symmetric boundary layer (i.e., a ring), the stellar photosphere occults roughly half of the boundary layer for most inclination angles. Approximately 50% of the optical excess emission from the models in § V comes from ultraviolet wavelengths that we did not observe spectrophotometrically. Hence, $L_{bl} \sim 3\ L_{uv/opt}$ (cf. Hartmann & Kenyon 1990).

The mass accretion rates found from the optical excess luminosities (R_* taken from KH, $M_* = 0.8\ M_\odot$) are listed in Table 5 and are typically $\sim 10^{-7}\ M_\odot\ yr^{-1}$. Basri & Bertout (1989) also estimated mass loss rates for AA Tau, BP Tau, DK Tau, DN Tau, and GG Tau from analysis of medium-resolution (3–7 Å) spectra; their mass-loss rates are on average a factor of ~ 3 lower than ours. This discrepancy is not surprising given the difficulty of determining the veiling precisely from medium-resolution spectra and given the variability of the objects.

The best estimate of the mass accretion rates for heavily veiled stars such as DR Tau is $\sim 10^{-6}\ M_\odot\ yr^{-1}$ (the r-values of DR Tau are ~ 10 times those of the stars listed in Table 2), although it is impossible to measure accretion rates for heavily veiled stars accurately without a knowledge of the reddening, the stellar radius, and the stellar spectral type. We estimate the mass accretion rates in Table 5 to be uncertain by $\sim 50\%$ for each object because of uncertain bolometric and geometric corrections.

Hartmann & Kenyon (1990) estimate that accretion from a circumstellar disk onto a T Tauri star will alter the evolutionary track of the star in the H-R diagram if the mass accretion rate exceeds a critical value of $\sim 9 \times 10^{-8}\ M_\odot\ yr^{-1}$. The mass accretion rates of most of our program objects are comparable to or greater than this critical value, suggesting that disk accretion plays a major role in the evolution of young stellar objects.

Several attempts have been made to infer accretion luminosities in T Tauri stars by computing the difference, $L_{acc} = L_{ir} - L_{rep}$ between infrared and reprocessing luminosities (Strom et al. 1988; Cohen et al. 1989; Cabrit et al. 1990). These estimates all suffer from the fact that L_{ir} for most T Tauri stars is comparable to the L_{rep} predicted from simple disk models (Adams et al. 1987). The reprocessing luminosity is proportional to the luminosity of the central star, so that small errors in L_* can translate into substantial errors in the accretion rate. The reprocessing component L_{rep} equals $0.25\ L_*$ for a flat, optically thick disk (Adams & Shu 1986) and can be as large as $\sim 0.45\ L_*$ if the disk flares (Kenyon & Hartmann 1987).

TABLE 5

EXCESS LUMINOSITIES AND MASS ACCRETION RATES

Object	$R/R_\odot$[a]	L_*	$L_{uv/opt}$ ($L_\odot$)	M_{acc}[b]	L_{acc}/L_{rep}[c]
AA Tau	2.5	1.3	0.11	0.7	0.8
	2.5	0.3	0.06	0.4	1.8
BP Tau	2.9	1.7	0.19	1.4	1.0
	2.9	1.3	0.15	1.1	1.0
CI Tau	2.9	1.4	0.18	1.3	1.2
DK Tau	3.1	1.9	0.26	2.0	1.2
DN Tau	1.6	2.1	0.07	0.3	0.3
GG Tau	3.4	2.4	0.19	1.6	0.7
	3.4	2.3	0.10	0.9	0.4
GI Tau	2.8	1.5	0.11	0.8	0.7
UY Aur	3.4	1.0	0.08	0.7	0.7
	3.4	1.0	0.07	0.6	0.6
	3.4	1.1	0.11	0.9	0.9

[a] Stellar radii taken from Kenyon & Hartmann 1990.

[b] The accretion rate $\dot{M}_{acc}$ in units $10^{-7}\ M_\odot\ yr^{-1}$, calculated using $\dot{M} = 2 \times 10^{-7}\,(R/R_\odot)(L_{uv/opt}/L_\odot)(M/M_\odot)^{-1}$, with $M = 0.8\ M_\odot$.

[c] The ratio of accretion luminosity to reprocessing luminosity, assuming $L_{acc} = 3\ L_{uv/opt}$ and $L_{rep} = 0.33\ L_*$.

6.3. *Infrared Excess Luminosities: Reprocessing or Accretion?*

The photospheric fluxes of the T Tauri stars can be extrapolated to infrared wavelengths (using the colors of the standard template) and compared with infrared photometry to estimate the amount of infrared excess emission present in these objects. The results appear in Figure 12. We use photometry obtained in 1988 October at San-Pedro Martir observatory to calculate the near-infrared excesses for BP Tau, GG Tau, and AA Tau, and observations by Rydgren & Vrba (1983) and Rydgren et al.

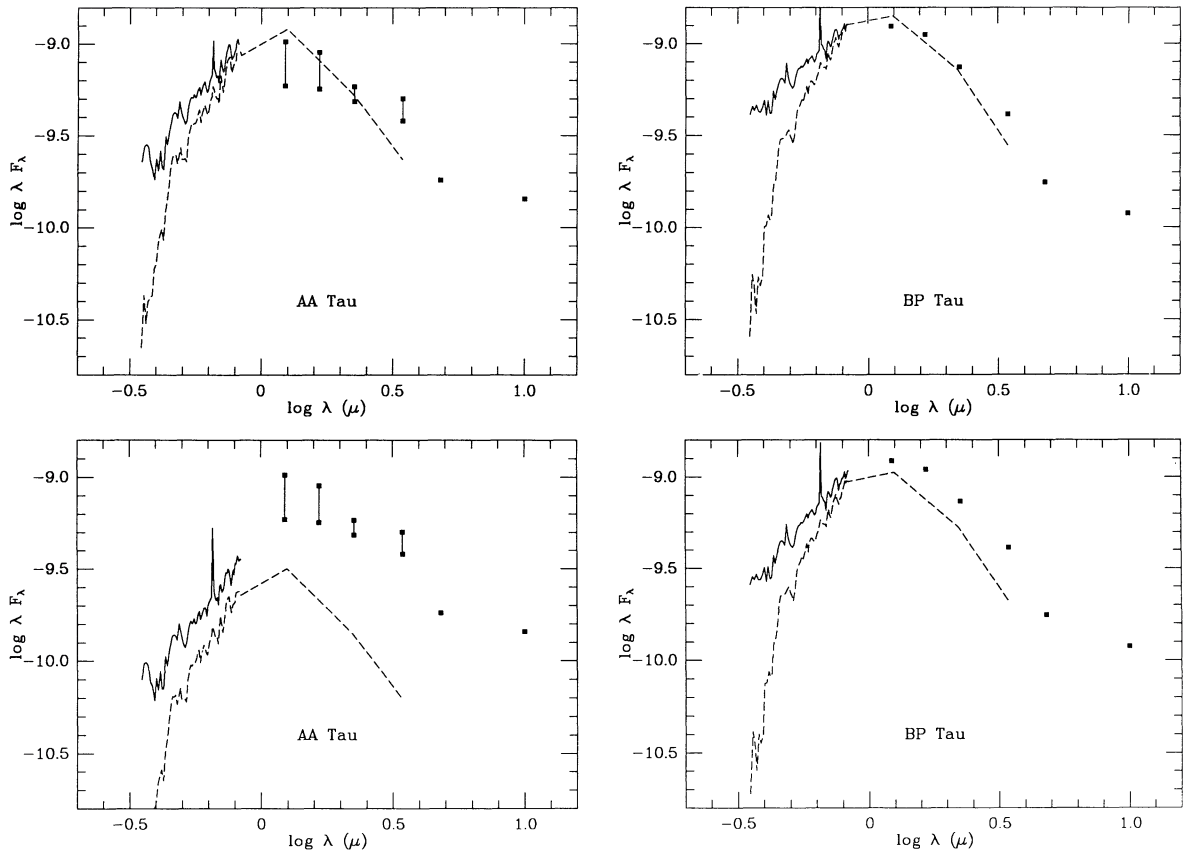

FIG. 12.—The infrared excesses of our program T Tauri stars. The observed reddening-corrected spectra of the T Tauri stars between 3500 and 8250 Å, including the excess emission, are shown as solid lines. The dotted lines depict the photospheric fluxes of the stars, dereddened and corrected for optical excess emission. The extrapolation of the photospheric spectra to near-infrared wavelengths uses the photospheric colors of the standard templates. The infrared photometry is taken from observations at San-Pedro Martir observatory in 1988 October, and from the compilations of Rydgren & Vrba (1983) and Rydgren et al. (1984). The vertical bars connecting the infrared points for AA Tau (San-Pedro Martir data) and DK Tau (Rydgren & Vrba 1983) indicate the range of variability observed for these objects.

(1984) for the other objects. The infrared photometry is not simultaneous with the optical data, but IR photometry obtained by J. Bouvier (private communication) within several days of our optical spectra agree well (± 0.1 mag) with our adopted values.

Figure 12 shows that only one of our program objects, UY Aur, has a significant infrared excess at 1.25 μm (J). This star has an infrared energy distribution that is flat in log (λF_λ), and excess emission occurs at all wavelengths. The infrared excesses in the remainder of the objects in Figure 12 arise from wavelengths 2.2 μm (K) and longer. The large amplitude variations of the photosphere of AA Tau make it impossible to determine the amount of infrared excesses without exactly simultaneous infrared observations.

We can estimate the ratio of the infrared excess L_{rep} caused by reprocessing to the infrared excess L_{acc} produced from a steady accretion disk as follows. Let $\hat{L}$ be the luminosity of the disk (accretion or reprocessing) estimated by multiplying the observed flux from the disk by $4\pi d^2$, where d is the distance to the source. $\hat{L}$ will be larger than L, the true disk luminosity, when the disk appears nearly pole-on, and $\hat{L}$ will be less than L when the disk is viewed nearly edge-on. An annulus of an accretion disk with radius r and width dr has a specific luminosity $L_\nu(\text{ann}) = 2(\pi I_\nu)(2\pi r\, dr)$. The observed flux of the annulus at a distance d is $I_\nu(2\pi r\, dr)\cos i/d^2$, so that $\hat{L}_\nu(\text{ann}) = 4\pi I_\nu(2\pi r\, dr)\cos i = 2\cos i L_\nu(\text{ann})$. This expression is independent of the radius of the annulus and holds for all frequencies ν. Hence,

$$\hat{L} = 2L\cos i\,, \tag{8}$$

where $\hat{L}$ is the observed energy flux from the disk multiplied by $4\pi d^2$, and L is the luminosity of the disk.

Therefore, the amount of infrared excess emission expected from a flared reprocessing disk is $\hat{L}_{rep} = (2\cos i) \times 0.33\, L_*$ (Kenyon & Hartmann 1987), and the amount of infrared excess expected from a steady accretion disk is $\hat{L}_{acc} = (2\cos i) \times 3\, L_{uv/opt}$ (§ 6.2 and eq. [8]). The ratios $L_{acc}/L_{rep}\,(= \hat{L}_{acc}/\hat{L}_{rep})$ in Table 5 indicate that the accretion and reprocessing contribute equally to the total near-infrared excess when r(5500 Å) ~ 0.6.

The maximum infrared excess occurs when the disk appears face-on to the observer ($i = 0$) and is given by

$$\hat{L}_{max} = \hat{L}_{acc}(i=0) + \hat{L}_{rep}(i=0) = 2 \times (3\, L_{uv/opt} + 0.33\, L_*) \tag{9}$$

To test whether or not the sum of L_{acc} and L_{rep} can account for the infrared excesses in our program objects, we compared the observed infrared excess L_{ir} (calculated from 1 to 100 μm using Rydgren et al. 1984 for the near-infrared excesses and Cohen et al. 1989 for the far-infrared excesses) with $\hat{L}_{max}$. UY Aur was the only object in Table 5 with an observed infrared excess ($L_{ir} = 2.5\, L_\odot$) greater than that expected from the sum of reprocessing and accretion components ($\hat{L}_{max} = 0.6$

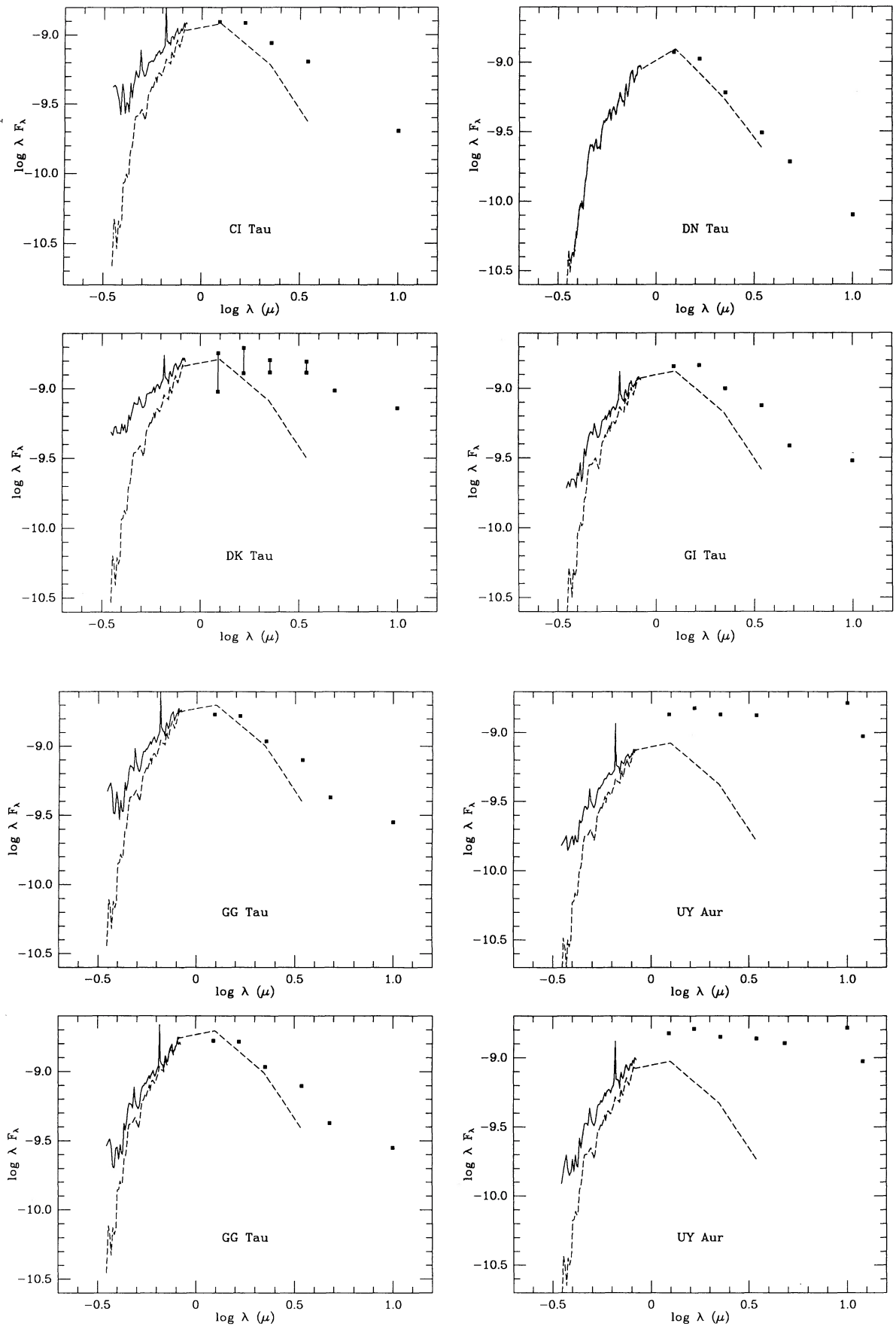

FIG. 12—*Continued*

$L_\odot$). The spectral energy distribution of UY Aur is flat in λF_λ and cannot be explained with a steady accretion disk or a simple reprocessing disk (e.g., Adams, Ruden, & Shu 1989). It is possible that some of the heavily veiled objects (Table 4) also have infrared excesses larger than expected from steady accretion and reprocessing, but we cannot estimate L_* (and hence, $\hat{L}_{max}$) for these objects because of the difficulty in measuring the reddening (§ 5.2).

7. SUMMARY

We have presented simultaneous high-resolution spectra and spectrophotometric observations of a sample of 22 weak-lined and classical T Tauri stars in the Taurus-Auriga dark cloud. The high-resolution spectra of T Tauri stars and standard stars enable us to separate the photospheric fluxes from the optical excess emission ("veiling") in our program objects, and we combine this information with the spectrophotometry to estimate the reddening, the stellar luminosities, variability, optical excess luminosities, and infrared excess luminosities of these stars.

We find that previous studies have systematically underestimated the extinction toward T Tauri stars by as much as 50% because they ignored the color changes introduced by the optical excess emission. Stellar luminosities calculated using the new extinction values agree with existing estimates that used near-infrared colors (J and H) for normalization. The variability of the T Tauri stars in our sample arises primarily from fluctuations in the amount of excess emission, but in at least one case (AA Tau), photospheric variations were equally important.

It is possible to extract a reddening-corrected spectrum of the optical excess emission without knowing the reddening to the veiled object a priori. The amount of optical excess emission ranges from undetectable ($\lesssim 0.1$ of the photosphere) to as much as 10 times the photospheric flux in the most extreme objects. The spectra of the excesses are flat in F_λ or rise slowly toward the blue at optical wavelengths, and must show Balmer jump emission. We modeled the observed spectral energy distribution of the excess emission with a slab of pure hydrogen gas in the constant temperature in LTE. The slabs have densities $\sim 10^{14}$ cm^{-3}, temperatures of ~ 9000 K, optical depths between ~ 0.8 and 4, and covering factors of $\sim 5\%$ of the stellar surface area to account for the observed Balmer emission jumps and the slopes of the optical continua. The parameters for the slab model are consistent with predictions from accretion disk models, and our results support the suggestion that optical excess emission in T Tauri stars comes from the boundary layer of an accretion disk. Our models cannot distinguish between an axially symmetric accretion "ring" and non–axially symmetric models such as an accretion "hot spot," however.

The mass accretion rates in partially veiled T Tauri stars are $\sim 10^{-7}\ M_\odot$ yr^{-1}, although the most heavily veiled objects may accrete at a rate as high as $\sim 10^{-6}\ M_\odot$ yr^{-1}. These accretion rates are comparable to or exceed the critical value of $\sim 9 \times 10^{-8}\ M_\odot$ yr^{-1} calculated by Hartmann & Kenyon (1990) for altering the evolutionary track of a T Tauri star in the H-R diagram. A steady accretion disk model indicates that roughly half of the near-infrared excess emission from a typical partially veiled T Tauri star comes from reprocessing of stellar radiation, with the remaining half arising from accretion energy. Only one of the seven partially veiled T Tauri stars observed, UY Aur, exhibits more near-infrared excess emission than expected from the sum of reprocessing and accretion components of an accretion disk. The spectral energy distribution of this object (and other flat spectrum sources) is not explained well by steady accretion disk models.

P. H. thanks Rob Hewett for his help in developing and modifying the software used to analyze the data in this paper. We are indebted to the staff of KPNO for a generous allocation of telescope time for this project, and for their assistance at the 0.9 and 4 m telescopes, and to the staff at San-Pedro Martir observatory for obtaining near-infrared observations. We acknowledge useful discussions with G. Basri, C. Bertout, J. Bouvier, and S. Cabrit concerning the nature of accretion disks and veiling. This research was sponsored in part by the Scholarly Studies program of the Smithsonian Institution.

REFERENCES

Adams, F. C., Emerson, J. P., & Fuller, G. A. 1990, ApJ, 357, 606
Adams, F. C., Lada, C. J., & Shu, F. H. 1987, ApJ, 312, 788
Adams, F. C., Ruden, S. P., & Shu, F. H. 1989, ApJ, 347, 959
Adams, F. C., & Shu, F. H. 1986, ApJ, 308, 836
Appenzeller, I., Jankovics, I., & Östreicher, R. 1984, A&A, 141, 108
Basri, G., & Batalha, C. 1990, ApJ, 363, 654
Basri, G., & Bertout, C. 1989, ApJ, 341, 340
Beckwith, S. V. W., Sargent, A. I., Chini, R. S., & Güsten, R. 1990, AJ, 99, 924
Bertout, C., Basri, G., & Bouvier, J. 1988a, ApJ, 330, 350
Bouvier, J. 1990, AJ, 99, 946
Bouvier, J., Bertout, C., Benz, W., & Mayor, M. 1986, A&A, 165, 110
Cabrit, S., Edwards, S., Strom, S. E., & Strom, K. M. 1990, ApJ, 354, 687
Cohen, M., Emerson, J., & Beichman, C. 1989, ApJ, 339, 455
Cohen, M., & Kuhi, L. V. 1979, ApJS, 41, 743
Durisen, R. H., Yang, S., Cassen, P., & Stahler, S. W. 1989, ApJ, 345, 959
Edwards, S., Cabrit, S., Strom, S. E., Heyer, I., Strom, K. M., & Anderson, E. 1987, ApJ, 321, 473
Hartigan, P., Hartmann, L., Kenyon, S. J., Hewett, R., & Stauffer, J. R. 1989, ApJS, 70, 899 (Paper I)
Hartigan, P., Hartmann, L., Kenyon, S. J., Strom, S. E., & Skrutskie, M. F. 1990, ApJ, 354, L25
Hartmann, L., Hewett, R., Stahler, S., & Mathieu, R. D. 1986, ApJ, 309, 275
Hartmann, L., & Kenyon, S. 1985, ApJ, 299, 462
Hartmann, L., & Kenyon, S. 1990, ApJ, 349, 190
Hartmann, L., & Stauffer, J. 1989, AJ, 97, 873
Herbig, G. H. 1977, ApJ, 214, 747
Herbig, G. H., & Goodrich, R. W. 1986, ApJ, 309, 294
Jacoby, G. H., Hunter, D. A., & Christian, C. A. 1984, ApJS, 56, 257
Kenyon, S. J., & Hartmann, L. 1987, ApJ, 323, 714
———. 1990, ApJ, 349, 197 (KH)
Lynden-Bell, D., & Pringle, J. E. 1974, MNRAS, 168, 603
Rucinski, S. M. 1985, AJ, 90, 2321
Rydgren, A. E., Schmelz, J. T., Zak, D. S., & Vrba, F. J. 1984, Pub. US Naval, Obs., 2d Ser., 25, 1
Rydgren, A. E., & Vrba, F. J. 1983, AJ, 88, 1017
Savage, B. D., & Mathis, J. D. 1979, ARA&A, 17, 73
Strom, K. M., Strom, S. E., Edwards, S., Cabrit, S., & Skrutskie, M. F. 1989, AJ, 97, 1451
Strom, K. M., Strom, S. E., Kenyon, S. J., & Hartmann, L. W. 1988, AJ, 95, 534
Vrba, F. J., Rydgren, A. E., Chugainov, P. F., Shakovskaya, N. I., & Weaver, W. B. 1989, AJ, 97, 483
Walker, M. F. 1987, PASP, 99, 392
Walter, F. M., Brown, A., Mathieu, R. D., Myers, P. C., & Vrba, F. J. 1988, AJ, 96, 297
Walter, F. M., & Kuhi, L. V. 1981, ApJ, 250, 254